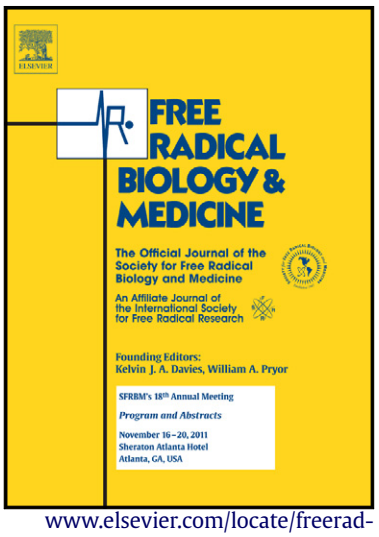

www.elsevier.com/locate/freerad-biomed

Insulin and IGF-1 improve mitochondrial function in a PI-3K/Akt-dependent manner and reduce mitochondrial generation of reactive oxygen species in Huntington's disease knock-in striatal cells

Márcio Ribeiro, Tatiana Rosenstock, Ana M. Oliveira, Catarina R. Oliveira, A. Cristina Rego

PII: S0891-5849(14)00275-5
DOI: http://dx.doi.org/10.1016/j.freeradbiomed.2014.06.023
Reference: FRB12057

To appear in: *Free Radical Biology and Medicine*

Received date: 15 November 2013
Revised date: 1 June 2014
Accepted date: 21 June 2014

Cite this article as: Márcio Ribeiro, Tatiana Rosenstock, Ana M. Oliveira, Catarina R. Oliveira, A. Cristina Rego, Insulin and IGF-1 improve mitochondrial function in a PI-3K/Akt-dependent manner and reduce mitochondrial generation of reactive oxygen species in Huntington's disease knock-in striatal cells, *Free Radical Biology and Medicine,* http://dx.doi.org/10.1016/j.freeradbiomed.2014.06.023

Insulin and IGF-1 improve mitochondrial function in a PI-3K/Akt-dependent manner and reduce mitochondrial generation of reactive oxygen species in Huntington's disease knock-in striatal cells

Márcio Ribeiro[1], Tatiana Rosenstock[1], Ana M. Oliveira[1], Catarina R. Oliveira[1,2], A. Cristina Rego[1,2*]

[1]CNC-Center for Neuroscience and Cell Biology, University of Coimbra and [2]Faculty of Medicine, University of Coimbra, 3004-504 Coimbra, Portugal

Running title: Insulin/IGF1 and mitochondria in HD

[*] To whom correspondence should be addressed:
Ana Cristina Rego (Ph.D.), Center for Neuroscience and Cell Biology, and Faculty of Medicine, Rua Larga University of Coimbra, polo I, 3004-504 Coimbra, Portugal.
Tel: +351-239-820190; Fax: +351-239-822776
E-mail: a.cristina.rego@gmail.com; acrego@cnc.uc.pt; arego@fmed.uc.pt.

Keywords:
Huntington disease; oxidative stress; insulin/IGF-1 signaling; Nrf2; mitochondria; reactive oxygen species; striatal cells, Akt.

Abstract

Oxidative stress and mitochondrial dysfunction have been described in Huntington's disease, a disorder caused by expression of mutant huntingtin (mHtt). IGF-1 was previously shown to protect HD cells, whereas insulin prevented neuronal oxidative stress. In this work we analysed the role of insulin and IGF-1 in striatal cells derived from HD knock-in mice on mitochondrial production of reactive oxygen species (ROS) and related antioxidant and signaling pathways influencing mitochondrial function. Insulin and IGF-1 decreased mitochondrial ROS induced by mHtt and normalized mitochondrial SOD activity, without affecting intracellular glutathione levels. IGF-1 and insulin promoted Akt phosphorylation without changing the nuclear levels of phosphorylated Nrf2 or Nrf2/ARE activity. Insulin and IGF-1 treatment also decreased mitochondrial Drp1 phosphorylation, suggesting reduced mitochondrial fragmentation, and ameliorated mitochondrial function in HD cells in a PI-3K/Akt-dependent manner. This was accompanied by increased total and phosphorylated Akt, Tfam and mitochondrial-encoded cytochrome c oxidase II, as well as Tom20 and Tom40 in mitochondria of insulin- and IGF-1-treated mutant striatal cells. Concomitantly, insulin/IGF-1-treated mutant cells showed reduced apoptotic features. Hence, insulin and IGF-1 improve mitochondrial function and reduce mitochondrial ROS caused by mHtt by activating the PI-3K/Akt signaling pathway, in a process independent of Nrf2 transcriptional activity, but involving enhanced mitochondrial levels of Akt and mitochondrial-encoded complex IV subunit.

Abbreviations: Akt, protein kinase B; ARE, antioxidant responsive element; Erk, extracellular signal-regulated kinase; CBP, CREB-binding protein; CREB, cAMP response-element (CRE) binding protein; CDK (cyclin-dependent kinase); DHE, dihydroethidium; Drp1, dynamin-related protein 1 or dynamin 1-like (DNM1L); GCL, glutamate-cysteine ligase; GCLc, glutamate-cysteine catalytic subunit; GPx, glutathione peroxidase; GSH, glutathione, reduced form; GSSG, glutathione oxidized form; IGF-1, Insulin-like growth factor 1; IGF1R, insulin-like growth factor 1 receptor; IR, insulin receptor; IRS, insulin receptor substrate; H_2DCFDA, 2',7'-dichlorodihydrofluorescein diacetate; HKII, hexokinase type II; HD, Huntington's disease; HO-1, heme oxygenase; Hsp60, heat shock 60kDa protein 1 (chaperonin); mHtt, mutant huntingtin;

mtDNA, mitochondrial DNA; MT-COII, mitochondrial-encoded cytochrome c oxidase II; mTOR, mammalian target of rapamycin; NDUFS3, NADH dehydrogenase (ubiquinone) Fe-S protein 3, 30kDa (NADH-coenzyme Q reductase); NQO1, NAD(P)H dehydrogenase [quinone] 1; Nrf2, nuclear factor (erythroid-derived 2)-like 2; PI-3K, phosphatidylinositol 3-kinase; PGC-1α, peroxisome proliferator-activated receptor-γ coactivator 1α; ROS, reactive oxygen species; SDHA, succinate dehydrogenase complex, subunit A, flavoprotein (Fp); SOD, superoxide dismutase; Tfam, transcription factor A, mitochondrial; TMRM, tetramethylrhodamine methyl ester; Tom20, translocase of outer mitochondrial membrane 20 homolog (yeast); Tom40, translocase of outer mitochondrial membrane 40 homolog (yeast).

Introduction

Huntington's disease (HD) is a progressive neurodegenerative disorder characterized by motor and psychiatric disturbances and cognitive decline leading to dementia. HD results from CAG repeat expansion in the *HD* gene, leading to increased polyglutamine tail at the N-terminal of huntingtin (Htt) [1]. The resultant mutant Htt (mHtt) causes striatal and cortical neurodegeneration, which has been linked to several pathological mechanisms, including excitotoxicity, proteasomal dysfunction, transcriptional deregulation, mitochondrial dysfunction, impaired energy metabolism and oxidative stress [2,3].

Several oxidative stress markers were previously observed in HD. Elevated levels of DNA oxidation were detected in blood plasma, serum and leukocytes from HD patients [4-6] and in striatum and cortex of HD *post-mortem* tissues [7-9]. DNA oxidation was also detected in the striatum, urine and plasma of R6/2 HD mice [10]. Increased lipid peroxidation markers were also detected in HD patient's blood serum and plasma, correlating with disease severity [5, 11] in the striatum and cortex of *post-mortem* HD human brains [12,13] and in total brain and striatum of R6/2 mice, co-localizing with mHtt inclusions [13,14]. Moreover, intracellular aggregates of mHtt exon-1 were directly linked to increased production of reactive oxygen species (ROS), in a polyglutamine length-dependent manner, preceding cell death [15]. Impairment in antioxidant defenses also underlies oxidative stress in HD. In erythrocytes from HD patients, glutathione peroxidase (GPx) and superoxide dismutase 1 (SOD1 or Cu/Zn-SOD) activities were decreased [5]. Proteomic analysis of HD *post-mortem* striatal and cortical brain samples revealed the induction of peroxiredoxins 1, 2 and 6 and GPx 1 and 6, and increased activities of SOD2 (Mn-

SOD) and catalase [16]. More recently, we demonstrated increased ROS formation and deregulated glutathione redox cycle in HD striatal cells [17].

ROS formation in HD has been largely attributed to impaired mitochondrial function. Evidences for mitochondrial dysfunction in HD include, among other reports, decreased activity of mitochondrial complexes I-IV in caudate and putamen, and in muscle and platelets of HD patients [e.g. 18,19], reduced activities of complexes I, IV and V in progenitor and differentiated neuron-like ST*Hdh*$^{Q111/Q111}$ cells [20], mitochondrial membrane depolarization and decreased mitochondrial Ca^{2+} retention [21,22]. ST*Hdh*$^{Q111/Q111}$ striatal cells also showed high levels of mitochondrial ROS, mitochondrial DNA (mtDNA) damage and a lower spare respiratory capacity [23]. Treatment with a mitochondria-specific antioxidant improved mitochondrial function in HdhQ150 knock-in mice and restored mtDNA copy number to levels similar to the controls [24]. These results suggest oxidative stress-induced mitochondrial abnormalities following mHtt expression. Interaction of mHtt with the outer mitochondrial membrane was further demonstrated in mitochondria from YAC72 transgenic mice, ST*Hdh*$^{Q111/Q111}$ striatal cells and in mouse liver mitochondria, causing the opening of the mitochondrial permeability transition pore [21,25].

Neuronal survival largely depends on growth factors through activation of kinases, namely the Ser/Thr protein kinase B (Akt). Insulin-like growth factor 1 (IGF-1) levels were decreased in HD mutant striatal cells, in human HD striatal *post-mortem* tissues and in plasma of 11 week-old R6/2 mice [26]. Moreover, IGF-1-mediated Akt activation was described to be neuroprotective in HD and to reduce nuclear inclusions through phosphorylation of mHtt at Ser421 [27]; activation of Akt was described to reflect early striatal pro-survival response in HD knock-in *Hdh*^{Q111} mice and ST*Hdh*$^{Q111/Q111}$ cells [28]. We previously reported that peripheral administration of IGF-1 protected against HD-associated impaired glucose tolerance in R6/2 mice [29]. Furthermore, we recently showed that intranasal administration IGF-1 in YAC128 mice enhanced IGF-1 cortical levels, improved motor activity, activated Akt, enhanced mHtt phosphorylation at Ser421 and improved brain metabolic features [30]. Insulin, which shares structural and signaling properties with IGF-1, also protected against oxidative stress in cortical neurons through Akt activation [31]. Interestingly, in endothelial cells, insulin induced the expression of glutamate-cysteine ligase (GCL) catalytic subunit (GCLc) through the transcription factor nuclear factor (erythroid-derived 2)-like 2 (Nrf2) [32], directly interfering with cellular antioxidant profile. Importantly,

impaired Nrf2 signaling pathway was recently described in striatal ST*Hdh*$^{Q111/Q111}$ cells [33]. Interestingly, insulin/IGF-1-related signaling kinases, namely Akt and extracellular signal-regulated kinase 1/2 (Erk1/2) were shown to translocate to the mitochondria and regulate several different proteins crucial to mitochondrial function. While Akt was described to promote enhanced mitochondrial function, Erk1/2 might conduce an opposite effect [e.g. 34-37].

In this work we examined the role of insulin and IGF-1 on mitochondrial ROS generation and mitochondrial membrane potential, and evaluated Nrf2 transcriptional activity related with antioxidant profile in HD knock-in striatal cells. We show that insulin and IGF-1 inhibit cellular Erk activation, increase Akt activation and Akt mitochondrial translocation, and enhance the levels of proteins involved in mitochondrial protein import, heighten mitochondrial function, and precluding mitochondrial ROS formation and cell death induced by mHtt.

Materials and Methods

Materials: DMEM culture medium and antibiotics were purchased by GIBCO (Paisley, UK). Anti-P(Thr308)Akt (ab38449), Anti-SOD1 (ab16831), anti-Ac(K68)SOD2 (ab137037), anti-SOD2 (ab13533), anti-GCLc (ab17926), anti-Nrf2 (ab31163), anti-P(Ser40)Nrf2 (ab76026), and anti-TBP (ab51841) were from Abcam (Cambridge, UK). LY294002 and antibodies against Akt (#9272), Erk1/2 (p44/42 MAPK) (#9102), P(Thr202/Tyr204)Erk1/2 (#4377), dynamin-related protein 1 (Drp1) or dynamin 1-like (DNM1L) (#8570), P(Ser616)Drp1 (#3455), and were from Cell Signaling Technology (Beverly, MA, USA). Anti-heat shock 60kDa protein 1 (chaperonin) (Hsp60) (#611562) was from BD Transduction Laboratories (San Jose, CA, USA). Anti-hexokinase type II (HKII) (AB3279) was from Chemicon (Merck Millipore, Billerica, MA, USA). Antibodies against translocase of outer mitochondrial membrane 20 homolog (yeast) (Tom20) (sc-11415) and translocase of outer mitochondrial membrane 40 homolog (yeast) (Tom40) (sc-11414) were from Santa Cruz Biotechnology (Santa Cruz, CA, USA). Hoechst 33342 nucleic acid stain and antibodies against mitochondrial-encoded cytochrome c oxidase II (MT-COII) (A-6404), NADH dehydrogenase (ubiquinone) Fe-S protein 3, 30kDa (NADH-coenzyme Q reductase) (NDUFS3) (A-21343/459130), and succinate dehydrogenase complex, subunit A, flavoprotein (Fp) (SDHA) (A-11142) were from Invitrogen/Molecular Probes (Life Technologies Corporation, Carlsbad, CA, USA). Secondary antibodies conjugated to alkaline phosphatase (anti-mouse, anti-rabbit, and anti-goat) were purchased from Amersham Biosciences

(Buckinghamshire, UK). First Strand cDNA Synthesis Kit (AMV) was obtained from Roche (Mannheim, Germany). GoTaq Flexi DNA Polymerase and dNTP Mix were obtained from Promega (Madison, WI, USA). 2',7'-dichlorodihydrofluorescein diacetate (H_2DCFDA), dihydroethidium, MitoSOX™ Red, Ac-DEVD-AFC (Caspase-3 Substrate VII, Fluorogenic) and tetramethylrhodamine methyl ester ($TMRM^+$) were obtained from Calbiochem (Merck Millipore, Billerica, MA, USA). Other reagents, anti-β-actin and anti-α-tubulin, insulin from porcine pancreas, IGF-1, NEM (N-ethylmaleimide), OPA (ortho-phthaldialdehyde), and U0126 were from Sigma Chemical Co. (St Louis, MO, USA).

Cell culture: Striatal cells derived from knock-in mice expressing normal Htt (ST*Hdh*$^{Q7/Q7}$ or wild-type cells; clone 2aA5) or homozygous to mHtt with 111 glutamines (ST*Hdh*$^{Q111/Q111}$ or mutant cells; clone 109-1A) were used. Striatal cells were kindly donated by Dr. Marcy E. MacDonald (Department of Neurology, Massachusetts General Hospital, Boston, USA). The cells were maintained as described previously [38]. Striatal cells were plated on poly-L-lysine coated glass coverslips, multiwell chambers or flasks 48 h before the experiments in order to allow the desired confluence. In some experiments, cells were pre-incubated for 30 min with 25 μM LY294002 or 10 μM U0126 before supplementing with insulin or incubating with IGF-1 (0.1-10 nM) for 24 h. In some experiments, cells were incubated with 500 μM H_2O_2 during 3 h.

Intracellular ROS measurements: After brief washing with PBS, striatal cells were incubated for 30 min with 20 μM H_2DCFDA, at 33ºC, in Krebs medium (in mM: 135 NaCl, 5 KCl, 0.4 KH_2PO_4, 1.8 $CaCl_2$, 1 $MgSO_4$, 20 HEPES and 5.5 glucose) at pH 7.4. H_2DCFDA is incorporated by the cells and hydrolysed by esterases to form H_2DCF, which is then converted to DCF by intracellular ROS [39]. Intracellular ROS were measured by following DCF fluorescence (488 nm excitation, 530 nm emission) at 33ºC, continuously, for 1 h, using a Microplate Spectrofluorometer Gemini EM (Molecular Devices, USA). Superoxide anion ($O_2^{\bullet-}$) formation was determined by using the fluorescence probe dihydroehidium (DHE) (Molecular Probes, Invitrogen). DHE is permeable to cell membrane and in cytoplasm it is converted to ethidium by $O_2^{\bullet-}$. Then, ethidium binds to DNA and emits fluorescence [40]. Briefly, 5 μM DHE dissolved in Krebs medium was incubated in cells during 1 h at 33ºC. Fluorescence measurements were taken during 1 h (518 nm excitation; 605 nm emission) in the presence or absence of 10 μM rotenone, a

mitochondrial complex I inhibitor, or antimycin A, a mitochondrial complex III inhibitor. Mitochondrial $O_2^{\bullet-}$ production levels were measured by using the fluorescent probe MitoSOX^{TM} Red. Briefly, striatal cells were washed in PBS, and then incubated with 2.5 μM MitoSOX^{TM} Red in Krebs medium during 10 min, at 33ºC. The fluorescence was taken during 1 h and 30 min at 33ºC with 510 nm excitation and 580 nm emission. In order to correct the DCF, DHE and MitoSOX^{TM} Red fluorescence values for variations in total protein content in the wells, cell protein in each well was quantified by the BioRad protein assay. The values were obtained as RFU (Relative Fluorescence Units) per minute per mg protein for each condition and then expressed as a percentage of wild-type cells.

Nuclear morphometric analysis: Cells were washed in Krebs medium and further incubated with Hoechst 33342 (4 μg/mL, a blue permeable fluorescent dye, which binds to DNA, to determine nuclear morphology) during 20 min, in the dark. Live cells were analyzed by fluorescence microscopy. Images from three different fields for each condition, in a total of four different experiments (run in duplicates) were acquired in a fluorescence microscope Axiovert 200M equipped with a LD Plan-Neofluar/40x/0.6 and an MRm Axiocam (Carl Zeiss, Jena, Germany). Images were acquired with Axiovision software and nuclei were counted using an ImageJ 1.47v (Wayne Rasband, National Institutes of Health, USA) plugin, which allowed the quantification of apoptotic and senescent nuclei accordingly to Filippi-Chiela and collaborators [41].

Measurement of SOD activity: Determination of SOD activity was performed accordingly to the SOD Assay Kit (Sigma). In order to measure SOD2 activity, 2 mM potassium cyanide (which inhibits SOD1) was added.

Caspase-3 activity: Caspase-3-like activity was determined using a fluorimetric substrate Ac-DEVD-AFC. Striatal cells were washed 2 times with PBS and then lysed at 4ºC with a buffer composed by (in mM): 25 HEPES, 2 $MgCl_2$, 1 EDTA, 1 EGTA, 2 DTT, 0.1 PMSF, and 1:1000 protease inhibitors and 0.04% Triton X-100 (pH 7.5). After scraping, a reaction buffer composed by (final concentrations in the well) 25 mM HEPES, 10% sucrose, 0.1% CHAPS, 2 mM DTT and 15 μM Ac-DEVD-AFC (pH 7.5), was added to the cell samples. The fluorescence was taken

during 1 h at 33ºC with 400 nm excitation and 505 nm emission. After the readings, cell samples were used to determine protein content by Bio-Rad protein assay. The values were obtained as RFU (Relative Fluorescence Units) per minute per mg protein for each condition and then expressed as a percentage of wild-type cells.

Measurement of glutathione levels by fluorimetry: The levels of reduced and oxidized glutathione (GSH and GSSG, respectively) were measured as described in [17]. Briefly, striatal cells were cultured during 48h at 33ºC. After incubation, the cells were washed twice in PBS and lysed in 15 mM Tris, pH 7.4, with 0.2% Triton X-100. GSH levels were measured in samples after the addition of OPA (1 mg OPA/ml methanol) and 100 mM NaH_2PO_4. After 15 min incubation, the fluorescence was measured using an excitation wavelength of 350 nm and an emission wavelength of 420 nm. The experimental procedure for GSSG was similar, although the samples were mixed for 30 min with NEM (5 mg NEM/ml methanol) which forms adducts with GSH. Then, the mixture was incubated for 15 min in 100 mM NaOH plus OPA (1 mg OPA/ml methanol), and the fluorescence was measured with excitation at 350 nm and emission at 420 nm in a Gemini EM microplate spectrofluorometer (Molecular Devices, USA). The results were calculated as RFU per milligram protein and expressed as percentage of wild-type control cells.

Subcellular fractionation: Cellular and nuclear-enriched fractions were obtained from cells that were washed twice in ice-cold PBS and scrapped in lysis buffer 1 (in mM: 10 HEPES, 10 NaCl, 3 $MgCl_2$, 1 EGTA, 1% Triton X-100, pH 7.5) supplemented with 50 mM NaF, 1.5 mM Na_3VO_4, 1 mM DTT, 1 mM PMSF and 1 μg/mL protease inhibitor cocktail (chymostatin, pepstatin A, leupeptin and antipain). The cellular homogenate was incubated at 4ºC (on ice) for 40 min and then centrifuged at 4,700 rpm, for 12 min (4ºC). The pellet was resuspended in buffer 2 (in mM: 25 HEPES, 300 NaCl, 5 $MgCl_2$, 1 EGTA, 20% glycerol, pH 7.4) supplemented with 50 mM NaF, 1.5 mM Na_3VO_4, 1 mM DTT, 1 mM PMSF and 1 μg/mL protease inhibitor cocktail, incubated on ice for 60 min, and further centrifuged at 10,600 rpm for 20 min (4°C). The resulting supernatant was collected and combined with the supernatant obtained from the first centrifugation (cellular fraction), whereas the resulting pellet (nuclear-enriched fraction) was resuspended in buffer 2. The samples were then frozen and thawed three times in liquid nitrogen, sonicated for 30 sec, and the samples were stored at −80 °C.

To obtain the cytosolic and mitochondrial-enriched fractions, striatal cells were washed with PBS and lysed at 4ºC using a sucrose buffer (pH 7.5) composed by (in mM): 250 sucrose, 20 HEPES, 100 KCl, 1.5 $MgCl_2$, 1 EDTA and 1 EGTA, 1 DTT, 1 PMSF, and 1 µg/mL protease inhibitor cocktail, homogenized by using a potter (120 strokes). The extracts were centrifuged at 800 g during 10 min in order to remove nuclear debris. The resulting supernatant was further centrifuged at 11,000 g for 10 min. Both the supernatant and pellet were collected into different centrifuge tubes. The supernatant was precipitated with acetone 100% and centrifuged at 12,000 g for 5 min. The resulting supernatant was discarded and the pellet was resuspended in sucrose buffer supplemented with 0.5% Triton X-100 (cytosolic fraction). The pellet obtained from the second centrifugation was resuspended in sucrose buffer and centrifuged at 11,000 g for 10 min. The resulting supernatant was discarded and the pellet was resuspended in sucrose buffer supplemented with Triton X-100 and further sonicated for 30 sec (mitochondrial fraction).

Western Blotting: Samples were denaturated in 50 mM Tris-HCl, pH 6.8, 2% sodium dodecyl sulphate (SDS), 5% glycerol, 0.01% bromophenol blue and 100 mM DTT at 95ºC, for 5 min. Equivalent amounts of 20-60 µg of protein were separated on 7.5%, 10% or 12% SDS-PAGE and electroblotted onto polyvinylidene difluoride (PVDF) membranes. The membranes were further blocked with 5% BSA and incubated with anti-GCLc (1:1000), anti-SOD1 (1:1000), anti-Ac(Lys68)SOD2 (1:1000), anti-SOD2 (1:1000), anti-Akt (1:1000), anti-p-(Thr308)Akt (1:500), anti-Erk (1:1000), anti-p-(Thr202/Tyr204)Erk (1:500), anti-Nrf2 (1:1000), anti-p-(Ser40)Nrf2 (1:500), anti-Hsp60 (1:1000), anti-HKII (1:1000), anti-Tfam (1:200), anti-Tom20 (1:200), anti-Tom40 (1:200), anti-NDUSF3 (1:1000), anti-MT-COII (1:1000), anti-HSP60 (1:1000), anti-Drp1 (1:1000), anti-p-(Ser616)Drp1 (1:500). Anti-β-actin (1:5000) was used as loading controls for total cellular and cytosolic fractions, while anti-TBP (TATA binding protein) (1:1000) and anti-SDHA (1:1000) were used as loading controls of nuclear and mitochondrial fractions, respectively. Immunoreactive bands were visualized by alkaline phosphatase activity after incubation with ECF reagent, by using a BioRad Versa Doc 3000 Imaging System. For membrane reprobing, a mild stripping buffer was used, consisting of 1.5% glycine, 0.1% SDS, 1% Tween20, with pH adjusted to 2.2. Band intensities were quantified and corrected for background using Image Studio Lite Software (LI-COR Biosciences, Lincoln, Nebraska, USA).

Luciferase gene reporter assay: Nrf2 transcription activity was measured based on its capability of binding the antioxidant responsive element (ARE), promoting luciferase gene transcription. Striatal cells plated on 12-well plates (90,000 cells/well) were transfected with the reporter construct [pGL4.37[luc2P/ARE/Hygro] (Promega) using Fugene 6 (Promega) by adding 1.1 μg plasmid. After 24 h, cells were exposed to insulin (0.1 nM) for another 24 h. 3 days after transfection, cells were washed with PBS and incubated at -80ºC for 2 h in Lysis Buffer (1.15 M Tris, 1 mM EDTA, 8 mM $MgCl_2$, 15% glycerol, 1 mM DTT, 1% Triton X-100, pH 7.4). Cells were then scraped and samples were centrifuged (5 min, 4ºC at 14,000 rpm). 50 μl of the supernatant were transferred to a white opaque 96-wells plate. The luciferase activity was measured in a Microplate Luminometer Reader LMax 384 (Molecular Devices, USA) using two different buffers: Reading Buffer (1.15 M Tris, 1 mM EDTA, 8 mM $MgCl_2$, 15% glycerol, 1 mM DTT, 2 mM ATP, pH 7.4) and Luciferase Buffer (167 μM; prepared in water with pH 8). In order to correct the luciferase activity, the protein content in each well was measured by the Bio-Rad protein assay (Bradford method). The percentage of luciferase activity was then normalized to controls (wild-type cells transfected without any treatment).

Total RNA extraction, cDNA conversion and RT-PCR: RNA from different samples was obtained with Trizol Reagent according to the manufacturer's protocol. Briefly, striatal cells were lysed with Trizol and were homogeneized with a pipette. The RNA was precipitated with isopropyl alcohol and the final pellet was resuspended with water DEPC (diethylpyrocarbonate) 0.01% (v/v). Before performing RT-PCR, the quality of RNA was verified through an electrophoresis in 1% agarose gel to check the ribosomal RNA subunits 18S and 28S. Then, the samples were incubated at 65ºC for 15 min, to avoid extensive secondary structure that may interfere with the annealing step and then were chilled on ice for 5 min. The concentration of RNA was measured and 1 μg was used to transcribe RNA into cDNA with First Strand cDNA Synthesis Kit (AMV). The reaction was as follow: 10 min at +25°C and 60 min at +42°C, for primer annealing and cDNA synthesis, respectively, 5 min at +99°C, for the denaturation of reverse transcriptase and then the samples were cooled to +4°C for 5 min.

Quantification of GCLc, HO-1 and NQO1 mRNA levels: The cDNA of each sample (10 ng) was amplified using sequence-specific primers to GCLc: forward (5'-3') ATG GGG CTG CTG

TCC CAA G; reverse (5'-3') GTA TGA GAG GAT CAC CCT AG; HO-1: forward (5'-3') GCT CAC GGT CTC CAG TCG CC; reverse (5'-3') CAC TGC CAC TGT TGC CAA C; NQO1: forward (5'-3') AGG CTC AGC TCT TAC TAG C; reverse (5'-3') ATT CAT TTT GTT GTT ATG GCA G. The normalization of the amplified product was performed in relation to the product of actin obtained in the same samples using as primers (5'-3') GGA GAC GGG GTC ACC CAC AC and (5'-3') AGC CTC AGG GCA TCG GAA CC, forward and reverse respectively. All reactions were performed using GoTaq Flexi DNA Polymerase (5x kit) and 10 mM dNTP Mix. The amplification reaction mixture (50 μl) contained 10 μl of the cDNA template, 1.5 mM of $MgCl_2$, 0.2 μM of each primer, 0.05 U Taq Pol. The thermal cycling conditions included 3 min at 94ºC, proceeding with 40 cycles of 94ºC for 30 s, 57ºC for 30 s and 72ºC for 45 s, followed by 72ºC for 10 min. The size of the PCR products was visualized in a 1.7% agarose gel and analyzed afterwards. GCLc, HO-1 or NQO1 mRNA levels were expressed in relation to actin.

Analysis of mitochondrial membrane potential: Mitochondrial membrane potential was determined using the cationic fluorescent probe $TMRM^+$, widely used as a fluorescent probe for measuring *in situ* mitochondrial membrane potential [42]. The experiments were performed accordingly to [43], with minor modifications. Briefly, cells were cultured in a 96-well plate during 48 h, at 33ºC. Then, striatal cells were washed twice in PBS and 300 nM $TMRM^+$ (diluted in Krebs medium) was incubated during 1 h, at 33ºC. After incubation, the basal fluorescence was taken during 5 min using a Microplate Spectrofluorometer Gemini EM (Molecular Devices, USA) (540 nm excitation and 590 emission). FCCP (2.5 μM) and oligomycin (2 μg/ml), which produced maximal mitochondrial depolarization, were added to cells and the fluorescence was taken during another 5 min. Results were expressed as the difference between the increase in $TMRM^+$ fluorescence upon addition of FCCP plus oligomycin and basal fluorescence values, and converted to percentage of wild-type (control) cells.

Statistical analysis: Statistical significance was determined by one-way or two-way ANOVA followed by the Bonferroni post-hoc test for multiple groups or by the Student's *t*-test for comparison between two Gaussian populations, as described in figure legends. Data were

expressed as the mean ± S.E.M. of the number of experiments indicated in figure legends. Significance was accepted at $p<0.05$.

Results

Insulin and IGF-1 prevent increased mitochondrial-driven ROS generation and apoptotic features in HD mutant striatal cells

Initially we determined the effect of insulin and IGF-1 on ROS formation in ST*Hdh*$^{Q111/Q111}$ cells. Due to structural and functional homology, insulin and IGF-1 can bind to (and activate) both insulin receptor (IR) and insulin-like growth factor 1 receptor (IGF1R), with insulin binding to the IR with higher affinity (< 1 nM) than IGF-1 (100–500-fold lower affinity), whereas IGF1R preferentially binds IGF-1 (< 1nM) as compared to insulin (100–500-fold lower affinity) [44]. Taking this into account, striatal cells were exposed to insulin or IGF-1 in the low nM range (0.1-10 nM).

Mitochondrial $O_2^{\bullet-}$ was measured using MitoSOX Red, a triphenylphosphonium cation conjugated with hydroethidine that readily reacts with $O_2^{\bullet-}$ [45], although it may also non-specifically oxidize [46]. Importantly, a significant increase in mitochondrial $O_2^{\bullet-}$ (Fig. 1A) was observed in HD knock-in striatal cells expressing full-length mHtt (ST*Hdh*$^{Q111/Q111}$ or mutant cells), when compared to ST*Hdh*$^{Q7/Q7}$ cells (wild-type cells). Enhanced levels of mitochondrial-generated $O_2^{\bullet-}$ in mutant cells were further revealed with the fluorescent probe hydroethidine following exposure to rotenone (complex I inhibitor) and antimycin A (complex III inhibitor) (Fig. 1B), thereby confirming increased production of mitochondrial ROS. When exposed to insulin or IGF-1, mutant cells presented a significant decrease in mitochondrial $O_2^{\bullet-}$ formation (Fig. 1A). Moreover, both insulin and IGF-1 significantly precluded the generation of other ROS in mutant cells (supplementary Fig. S1A,B), as assessed with the fluorescent redox probe H_2DCFDA, which can be oxidized by hydroperoxides, peroxynitrite ($ONOO^-$), hydroxyl radicals ($^{\bullet}OH$) or hypochlorous acid, among other oxidants, and redox-active metals such as iron [46]. These data show that both insulin and IGF-1 (at low nM) preclude mHtt-induced generation of ROS, in particular mitochondrial $O_2^{\bullet-}$.

Because caspase-3 activation was previously observed in HD striatal cells [17,47,48], correlating with nuclear apoptotic features [49], we determined the effect of insulin and IGF-1 on caspase-3 activation and nuclear morphology, namely apoptotic and senescent nuclei, in mutant

versus wild-type cells. Insulin (0.1 nM) significantly protected against caspase-3 activation in mutant cells (Fig. 2A), whereas both insulin and IGF-1 (0.1 nM) largely reduced apoptotic and senescent nuclei induced by expression of mHtt (Fig. 2C). Notably, no changes in caspase-3 activity or apoptotic and senescent nuclei were observed in wild-type cells treated with insulin or IGF-1 (Fig. 2A,B).

Full-length mHtt modifies SOD1/2, GCL catalytic and glutathione levels – influence of insulin and IGF-1

In order to examine whether elevated levels of ROS in mutant cells, namely $O_2^{\bullet-}$, were due to alterations in antioxidant activities, we determined SOD1/2 activities and protein levels. A significant increase in SOD2 activity was observed in total cell extracts from mutant, compared to wild-type cells (Fig. 3A), suggesting a compensatory mechanism against high levels of mitochondrial $O_2^{\bullet-}$. Concordantly, SOD2 activity was increased in mitochondrial fractions from mutant cells (Fig. 3B). Since acetylation of SOD2 at Lys68 was reported to decrease its activity [50], we measured the acetylation levels of SOD2 in striatal cells. In agreement with increased SOD2 activity, we detected a decrease in Ac-SOD2/SOD2 ratio in mutant cells (Fig. 3C). Interestingly, a decrease in SOD2 protein levels was also verified in mutant cells (Fig. 3D). Exposure to insulin induced a significant increase in SOD2 acetylation levels in mutant cells (Fig. 3C), whereas IGF-1 increased SOD2 protein levels (Fig. 3D) without changing protein acetylation in mutant cells (Fig. 3C). We also observed increased activity of SOD1 in total (Fig. 3E) and mitochondrial (Fig. 3F) fractions; however no differences in SOD1 protein levels were detected in mutant *versus* wild-type cells (Fig. 3G). Moreover, both insulin and IGF-1 significantly decreased mitochondrial SOD (1 and 2) activities in mutant cells (Fig. 3H). These results indicate that increased ROS caused by expression of full-length mHtt largely correlate with increased SOD1 and 2 activities and that treatment with insulin or IGF-1 precluded the increase in SOD activity.

We previously showed that the activity of enzymes of the glutathione redox cycle were enhanced, whereas GCL and glutathione synthetase (GS) activities and protein levels of GCLc were decreased in HD mutant striatal cells [17]. Therefore, we determined the effect of insulin and IGF-1 on GCLc protein levels. GCLc levels were significant decrease in mutant cells, when compared to wild-type cells (Fig. 4A,B). Treatment with 0.1 nM insulin increased GCLc levels in

mutant cells, whereas IGF-1 (0.1 and 1 nM) increased GCLc levels in wild-type cells only, compared to non-treated conditions (Fig. 4A,B). A rise in glutathione levels in mutant cells, despite decreased GCL activity, was previously demonstrated [17]. Therefore, we tested whether insulin or IGF-1 could alter GSH and GSSG levels. Insulin slightly increased GSH and GSSG in wild-type cells, however, neither insulin nor IGF-1 altered GSH or GSSG levels in mutant cells (Fig. 4C,D). These data indicate that insulin ameliorates GCLc protein levels, although not affecting GSH or GSSG levels in cells expressing mHtt.

Insulin and IGF-1 enhance phosphorylated Nrf2 nuclear levels, but do not affect its transcriptional activity in HD striatal cells

In order to evaluate whether antioxidant response was induced by insulin and/or IGF-1, we analysed the levels of the transcription factor Nrf2, which is responsible for the transcription of many antioxidant enzymes, including SOD1 and GCLc, and thus is directly implicated in cellular detoxifying systems [32,51]. Human Nrf2 contains 605 amino acids with a predicted relative molecular mass (M_r) of 66 kDa (57 kDa in mice). However, it was shown that transcription and translation of the full-length Nrf2 cDNA produces a band at 66 kDa and a higher M_r band at approximately 96 kDa, likely due to the abundance of acidic residues in Nrf2 [52]. Lau and collaborators [53] have recently reported that the biologically relevant M_r of Nrf2 ranges from ~95-110 kDa. Indeed, we detected a strong band around 100 kDa for phosphorylated p-(Ser40)-Nrf2 in both cellular and nuclear fractions obtained from striatal cells. However, in the case of Nrf2 two bands of ~57 kDa and ~90 kDa were detected in cellular fractions, whereas a single band of ~90 kDa appeared in the nuclear fraction. In the present study we quantified the ~100 kDa band for p-(Ser40)-Nrf2 and the ~90 kDa band for Nrf2.

Protein kinase C phosphorylates Nrf2 at Ser40, leading to Nrf2 dissociation from its endogenous inhibitor Kelch-like ECH associated protein 1 (Keap1), which results in nuclear translocation of Nrf2 in response to oxidative stress [54]. Therefore, we measured the levels of p-(Ser40)-Nrf2/Nrf2 in both cellular and nuclear extracts of striatal cells. Phosphorylated p-(Ser40)-Nrf2/Nrf2 ratio in cellular fractions did not differ significantly between both cell types (wild-type and mutant) (Fig. 5A,B). In nuclear-enriched fractions derived from mutant cells, p-Nrf2/Nrf2 ratio was increased (Fig. 5C,D) when compared to wild-type cells; however, this did not correlate with Nrf2/ARE transcriptional activity, which was significantly decreased in HD

cells (Fig. 5E). The oxidant H_2O_2, used as a positive control to induce the oxidation of Keap1 cysteine residues and Nrf2 dissociation from Keap1 [55], increased both cellular and nuclear p-Nrf2/Nrf2 ratio levels in both striatal cells, although it only reached statistical significance in nuclear fractions from wild-type cells (Fig. 5A-D). Incubation of wild-type cells with 0.1 nM insulin or IGF-1 significantly increased nuclear p-Nrf2/Nrf2 ratio (Fig. 5C,D) and insulin enhanced Nrf2/ARE activity (Fig. 5E). However, exposure to insulin or IGF-1 did not alter p-Nrf2/Nrf2 in cellular or nuclear fractions, or Nrf2/ARE transcriptional activity in mutant cells (Fig. 5A-E).

In the nucleus Nrf2 activates the transcription of genes involved in antioxidant defense, including GCLc, NAD(P)H dehydrogenase [quinone] 1 (NQO1), heme oxygenase (HO-1), among others [51]. In order to examine the importance of Nrf2 in regulating the oxidant status in mutant cells and since we detected increased GCLc protein levels following insulin treatment, we determined the levels of mRNA of GCLc, NQO1 and HO-1 under basal conditions and after exposure to insulin and IGF-1 (Supplementary Fig. S2). In agreement with the decrease in Nrf2/ARE transcriptional activity and GCLc protein levels in untreated mutant cells, we observed a significant reduction in GCLc mRNA levels in HD knock-in cells, when compared to wild-type cells (Fig. S2A). No significant changes in GCLc mRNA levels were observed after treatment with 0.1 nM insulin or IGF-1 (Fig. S2B), concordantly with insulin inefficiency in promoting Nrf2 transcriptional activity (Fig. 5E). NQO1 and HO-1 mRNA were not significantly altered in untreated mutant *versus* wild-type cells, or after exposure to insulin or IGF-1 either (Fig. S2C-F).

Data suggest that mHtt-induced increased ROS is linked to increased nuclear Nrf2 phosphorylation, but reduced Nrf2-dependent transcriptional activity of antioxidant defense systems, which may further enhance the cellular levels of ROS (Fig. 1, S1). Although insulin and IGF-1 induced nuclear translocation of p-Nrf2 and transcriptional activation in wild-type cells, in the presence of mHtt Nrf2 activity was not stimulated by insulin or IGF-1 treatments, indicating that insulin- and IGF-1-induced protection against ROS formation in HD striatal cells is independent of Nrf2-regulated antioxidant response.

Insulin and IGF-1 ameliorate mitochondrial membrane potential via the PI-3K/Akt pathway in mutant cells

Because insulin and IGF-1 are able to stimulate intracellular signaling pathways, we next investigated the role of PI-3K/Akt and Erk in regulating an upstream pathway of cell survival linked to increased mitochondrial function. We measured total and phosphorylated levels of Akt, and Erk42/44 in wild-type and HD striatal cells, in the absence or presence of 0.1 nM insulin or IGF-1 (Fig. 6).

Expression of mHtt *per se* significantly decreased the ratio of cytosolic phosphorylated p-(Thr308)Akt/total Akt, and total Akt/actin, without changing cellular p-(Thr202/Tyr204)Erk(42/44)/total Erk(42/44) or total Erk(42/44) levels (Fig. 6A-F), indicating decreased activation of phosphatidylinositol 3-kinase (PI-3K)/Akt signaling pathway. We analysed p-(Thr308)Akt, which is phosphorylated by phosphoinositide-dependent protein kinase 1 (PDPK1), since it was described to better correlate with Akt protein kinase activity [56]. Exposure to 0.1 nM insulin or IGF-1 significantly increased p-(Thr308)Akt/total Akt (Fig. 6A,C), whereas both stimuli significantly decreased total Akt/actin (Fig. 6B,C) in both striatal cells, and decreased cellular p-(Thr202/Tyr204)Erk(42/44)/total Erk(42/44) ratio in mutant cells (Fig. 6D,F). No changes were verified in total Erk(42/44) levels with either insulin or IGF-1 stimuli in both striatal cells (Fig. 6E,F). Because Akt can activate mammalian target of rapamycin (mTOR) [57], we also analyzed the levels of p-(Ser2448)mTOR/mTOR; however, no significant effects were observed in the presence of insulin or IGF-1 in both striatal cells (data not shown). These results suggest that insulin and IGF-1 may regulate pro-survival responses in mutant striatal cells by activating Akt.

Akt also phosphorylates cAMP response-element (CRE) binding protein (CREB), promoting CBP recruitment to initiate gene transcription [58]. HD has been linked to dysregulation of CREB/CRE transcription leading to decreased activity of PGC-1α (peroxisome proliferator-activated receptor-γ co-activator 1α), a transcriptional regulator of mitochondrial biogenesis and antioxidant enzymes [59]. mHtt also interacts with and sequesters CBP within protein aggregates [60,61]. Analysis of CBP and PGC-1α in nuclear-enriched fractions from wild-type and mutant striatal cells revealed no significant differences after treatment with 0.1 nM insulin or IGF-1 (data not shown), indicating that CBP and PGC-1α are not affected by insulin or IGF-1.

Taking into account that insulin and IGF-1 protected from mitochondrial $O_2^{\bullet-}$ generation induced by expression of mHtt (Fig. 1), we next tested whether insulin and IGF-1 influenced mitochondrial fragmentation and function.

mHtt was previously described to bind Drp1, increasing its activity [62,63]. Drp1 is a cytosolic protein that translocates to the outer mitochondrial membrane to promote mitochondrial fragmentation. Phosphorylation of Drp1 at Ser616 is a target of several kinases, including Erk1/2, and was shown to enhance Drp1 activity, resulting in mitochondrial fragmentation [64]. In order to verify if Drp1 is actively increased in mutant cells, we measured the levels of p-(Ser616)Drp1 and total Drp1 in mitochondrial fractions. We observed increased p-(Ser616)Drp1/Drp1 in the mitochondria of mutant cells, compared to wild-type cells (Fig. 7A,C), despite decreased levels of Drp1 (Fig. 7B,C), suggesting increased mitochondrial fragmentation upon expression of mHtt. Treatment with insulin or IGF-1 significantly decreased mitochondrial p-(Ser616)Drp1/Drp1 in mutant cells (Fig. 7A,C), without affecting Drp1 levels (Fig. 7B,C). These data suggest that insulin and IGF-1 decrease mHtt-induced mitochondrial fragmentation.

Mitochondrial membrane potential, measured with $TMRM^+$ after complete depolarization with FCCP plus oligomycin, was decreased by almost 50% in mutant cells (Fig. 7D), revealing increased mitochondrial depolarization induced by mHtt. Both insulin and IGF-1 (0.1 nM) significantly increased mitochondrial membrane potential in mutant cells (Fig. 7D). Considering that SODs dismutate mitochondrial $O_2^{\bullet-}$ into H_2O_2, we verified whether increased ROS levels affected mitochondrial membrane potential in mutant striatal cells by analyzing the effect of exposure to H_2O_2 (500 μM, for 3 h). H_2O_2 greatly induced mitochondrial depolarization in both striatal cells (Fig. 7E). These data show that insulin and IGF-1 improve mitochondrial function, which appears to be in accordance with the decrease in mitochondrial ROS formation observed in HD striatal cells.

Because insulin and IGF-1 induced Akt activation and significantly decreased mitochondrial depolarization, compared to untreated mutant cells, we further tested whether the PI-3K/Akt pathway was involved in improving mitochondrial function in mutant cells, by testing the effect of LY294002, a highly selective inhibitor of PI-3K [65]. LY294002 (25 μM) decreased p-(Thr308)Akt/total Akt and thus Akt activation, as determined by western blotting (data not shown). No significant changes in mitochondrial membrane potential were observed in both striatal cells after treatment with LY294002 (Fig. 7F,G). However, insulin and IGF-1-evoked

increase in mitochondrial membrane potential was completely abrogated by LY294002 in mutant cells (Fig. 7G), whereas no changes were observed in wild-type cells (Fig. 7F). Thus, insulin and IGF-1 largely improve mitochondrial function through the PI-3K/Akt pathway in HD mutant cells.

In order to verify if insulin and IGF-1-induced increased mitochondrial membrane potential was dependent on Erk(42/44) activation, we tested the effect of U0126, an inhibitor of MEK/Erk activity [66]. U0126 (10 μM) decreased p-(Thr202/Tyr204)Erk(42/44)/total Erk(42/44) and thus Erk activation, as determined by western blotting (data not shown). U0126 *per se* caused a significant increase in mitochondrial membrane potential in both wild-type and mutant striatal cells (Fig. 7H,I); moreover, incubation with U0126 enhanced mitochondrial membrane potential in IGF-1-treated mutant cells (Fig. 7I).

Insulin and IGF-1 modify the levels of several proteins in mitochondria derived from mutant striatal cells

In order to further investigate PI-3K/Akt-dependent improvement in mitochondrial function evoked by insulin and IGF-1 in HD striatal cells (Fig. 7G), we next measured p-(Thr308)Akt and Akt levels in mitochondrial fractions of striatal cells. We used succinate dehydrogenase complex, subunit A, flavoprotein (Fp) (SDHA) protein for western blotting normalization, since it was the less variable protein found in mitochondrial fractions. Under basal/unstimulated conditions mitochondrial p-Akt(Thr308) levels were slightly decreased in mutant cells (Fig. 8A,L). Treatment with insulin or IGF-1 increased p-(Thr308)Akt and total Akt levels in mitochondria derived from mutant cells, whereas in wild-type cells only IGF-1 had a similar effect (Fig. 8A,B,L). Enhanced Akt protein levels in mitochondria (Fig. 8B) appear to correlate with decreased cytosolic Akt (Fig. 6B) after treatment with insulin or IGF-1.

Since the inhibitor of MEK/Erk signaling showed increased mitochondrial membrane potential in both striatal cells (Fig. 7H,I), we also analysed the levels of mitochondrial p-(Thr202/Tyr204)Erk(42/44) and total Erk(42/44). We verified a dramatic increase in the levels of mitochondrial p-(Thr202/Tyr204)Erk(42/44) in mutant cells compared to wild-type cells (Fig. 8C,L), but no changes observed for total Erk(42/44) levels (Fig. 8D,L). Neither insulin nor IGF-1 were able to reduce Erk(42/44) activation in mitochondria of mutant cells, while IGF-1 only decreased Erk(42/44) activation in wild-type cells (Fig. 8C,L).

Akt was described to phosphorylate hexokinase II (HKII) at Thr473, increasing HKII association with mitochondria and resulting in protection against H_2O_2 treatment [67]. Following treatment with insulin and IGF-1, mitochondrial HKII levels increased in both striatal cells, however it only reached significance in the case of IGF-1 (Fig. 8E,L). Heat shock 60kDa protein 1 (chaperonin) (Hsp60) was shown to directly interact with Akt1 resulting in its activation [68]. Mutant cells displayed significant reduced mitochondrial Hsp60, when compared to wild-type cells, while treatment with IGF-1, in particular, promoted increased Hsp60 levels in both striatal cells (Fig. 8F,L).

Because insertion of nuclear-encoded proteins in mitochondria largely depends on the presence of Tom20 (translocase of outer mitochondrial membrane 20) or Tom40 (translocase of outer mitochondrial membrane 40), among other translocases, we determined their protein levels in mitochondrial fractions derived from striatal cells. Tom20 was significantly decreased in mutant cells (Fig. 8G,L), suggesting deficits in the recognition and movement of cytosolically synthesized mitochondrial preproteins; importantly, this difference was alleviated after incubation with insulin and IGF-1 (Fig. 8G,L). Both peptides also enhanced mitochondrial Tom40 levels in wild-type cells (Fig. 8H,L), whereas insulin only increased Tom40 levels in mitochondria of mutant cells (Fig. 8H,L). These data suggest that insulin might induce increased mitochondrial import of preproteins.

Finally, we determined the influence of insulin and IGF-1 on mitochondrial levels of mitochondrial transcription factor A (Tfam), involved in mtDNA transcription and replication, in mitochondria derived from mutant and wild-type striatal cells. In previous studies the exogenous oxidant *t*-butyl hydroperoxide (*t*-BOOH) induced Akt activation, which in turn directly phosphorylated nuclear respiratory factor 1 (NRF-1) leading to its nuclear translocation and binding to Tfam promoter, resulting in its transcription [69]. Tfam levels were significantly decreased in mitochondria of mutant cells (Fig. 8I,L). In HD cells, insulin slightly increased, while IGF-1 greatly enhanced mitochondrial Tfam levels (Fig. 8I,L). To check whether increased Tfam in mitochondria correlated with modified mitochondrial DNA-encoded proteins, we analysed the protein levels of NADH dehydrogenase (ubiquinone) Fe-S protein 3, 30kDa (NADH-coenzyme Q reductase) (NDUSF3), a nuclear-encoded complex I subunit, and cytochrome c oxidase II (MT-COII), a mitochondrial-encoded complex IV subunit, in mitochondrial fractions derived from striatal cells. Under basal conditions there were no

differences in NDUSF3 or MT-COII protein levels (Fig. 8J,K,L). No changes in NDUSF3 were detected in mutant cells after treatment with insulin or IGF-1 (Fig. 8J,L) either. Conversely, treatment with insulin or IGF-1 promoted a significant increase in MT-COII protein levels particularly in mitochondria of mutant cells (Fig. 8K,L).

These data suggest that insulin and IGF-1 enhance the protein levels of several proteins related with increased mitochondrial function in HD cells, which may occur through the translocation of cytosolic proteins to the mitochondria and/or possible Akt-mediated phosphorylation of target proteins; moreover, increased mitochondrial Tfam levels correlate with enhanced levels of mitochondrial-encoded complex IV subunit in mutant cells exposed to insulin or IGF-1.

Discussion

Here we show that expression of full-length mHtt increases mitochondrial $O_2^{\bullet-}$ generation and impairs Nrf2 transcriptional activity resulting in decreased GCLc mRNA and protein levels. Nevertheless, neither insulin nor IGF-1 influence the expression of Nrf2-target genes (GCLc, NQO1 and HO-1) in HD striatal cells. Moreover, exposure of HD striatal cells to insulin and IGF-1 stimulate PI-3K/Akt pathway, promoting restoration of mitochondrial function, which correlate with decreased mitochondrial $O_2^{\bullet-}$ production and cell death. Importantly, insulin and IGF-1 reduce Drp1 activity, suggesting decreased mitochondrial fragmentation. Translocation of Akt to mitochondria and increased mitochondrial Akt activity, along with enhanced levels of mitochondrial proteins, namely HKII, Hsp60, Tom 20 and Tom40, Tfam and MT-COII, appear to mediate the protective effects induced by insulin and IGF-1.

Increased mitochondrial generation of ROS in HD striatal cells was accompanied by increased activities of SOD1/2, which was confirmed by reduced SOD2 acetylation. Treatment with insulin and IGF-1 reduced ROS levels and restored the activity of mitochondrial SOD activity in mutant cells, indicating diminished antioxidant response. Interestingly, insulin even promoted increased SOD2 acetylation, correlating with lower mitochondrial SOD activity, whereas IGF-1 increased SOD2 protein levels without changing its acetylation. An increase in SOD activity was previously observed in R6/1 HD mice at 19 weeks of age, although older mice exhibited decreased SOD activity [70]. Reduced activity of SOD1 was also observed in cortex and cerebellum of *post-mortem* human brain tissues [7] and in erythrocytes [5] of HD patients. In

a previous study we demonstrated increased ROS levels and decreased GCL activity, despite increased glutathione levels in HD striatal cells, which occurred as a result of a lower capacity of multidrug resistance-associated protein 1 (Mrp1) to export GSH to the extracellular space [17]. Although we detected increased p-Nrf2/Nrf2 nuclear levels in HD striatal cells, in contrast to van Roon-Mom and collaborators [71] we did not observe activation of Nrf2-responsive genes upon expression of mHtt under non-stimulated conditions. Indeed, Nrf2/ARE transcriptional activity was decreased in HD knock-in striatal cells, which was related with reduced mRNA and protein levels of GCLc. While insulin moderately enhanced GCLc protein levels in mutant striatal cells, no changes in GCLc expression were observed and glutathione levels remained unchanged, largely suggesting that ROS protection induced by insulin or IGF-1 is independent on glutathione antioxidant response. Moreover, expression of other Nrf2-target genes, such as HO-1 and NQO1, was not affected by insulin or IGF-1 either. Acetylation of Nrf2 by CREB-binding protein (CBP) was previously described to increase Nrf2 promoter-specific DNA binding [72]. Therefore, we hypothesize that insulin or IGF-1 may not be able to increase Nrf2 acetylation and promote its activity and/or may not efficiently bind to ARE due to the presence of mHtt in the nucleus.

We previously showed that HD striatal cells exhibit features of intrinsic apoptosis [48]. Enhanced caspase-3 activation has been linked to increased mitochondrial ROS formation. Indeed, we showed that there is a close interplay between endogenous ROS generation and caspase-3 activation in apoptotic neurons [43,73]. Both insulin and IGF-1 lowered the number apoptotic and senescent nuclei in mutant cells and prevented ROS generation in mutant cells, while insulin only was able to prevent caspase-3 activation in cells expressing mHtt. This may account for by differential activation of pro-survival signaling pathways in knock-in HD striatal cells exposed to insulin or IGF-1. Previously we demonstrated that insulin (at microM concentrations, potentially activating both insulin and IGF-1 receptors) can act as an antioxidant in cortical neurons, under conditions involving activation of Akt and inhibition of glycogen synthase kinase 3 beta (GSK3β) [31,74]. Indeed, unstimulated HD knock-in striatal cells showed reduced activation of PI-3K/Akt signaling pathway, which was stimulated by IGF-1 and insulin. Reduced Akt was previously reported in HD patients, appearing as a shorter inactive caspase-3-cleaved form [27,75]. Corroborating our study, p-(Ser473)Akt/Akt levels were significant decreased in ST*Hdh*$^{Q111/Q111}$ cells [76], in HEK293 cells expressing mHtt with 68 CAG repeats [77] and in HD patient's lymphoblasts and lymphocytes [75]. Akt activation is an early pro-

survival striatal response in knock-in *Hdh*^{Q111} mice and ST*Hdh*$^{Q111/Q111}$ cells [28]; importantly, activation of IGF-1/Akt pathway caused Htt phosphorylation at Ser421, decreasing mHtt nuclear inclusions and mHtt toxicity [27] and regulated anterograde and retrograde transport defects in HD cortical neurons [78]. Another study demonstrated that p-(Ser473)Akt was unchanged in YAC128 and in R6/2 HD mice, but the levels of p-(Ser421)Htt were decreased in the striatum of YAC128 mice and in cells expressing mHtt [79]. In contrast, insulin receptor substrate (IRS)-2, which activates PI-3K/Akt and mTOR cascade, promoted mitochondrial dysfunction and oxidative stress in R6/2 mice; however, in the same study, the authors showed that IRS-2 protein levels were unchanged in the striatum of patients with grade II HD [80]. Conversely, IRS-2 activation induced by insulin, IGF-1 and interleukin-4 enhanced exon1Htt clearance in a dose-dependent manner [81]. Thus, different IRS signaling pathways might be activated upon exposure to low nM insulin or IGF-1.

Plasma IGF-1 levels were previously shown to be reduced in HD patients, compared with controls [82], but higher IGF-1 in plasma correlated with cognitive decline in HD patients [83]. However, in another study, reduced IGF-1 mRNA was observed in striatum and skin fibroblasts of HD patients and HD knock-in striatal cells, and decreased plasma IGF-1 levels correlated with decreased body weight in R6/2 HD mice [26]. Additionally, we previously described that recombinant human IGF-1 (rhIGF-1) rescued peripheral metabolic abnormalities linked to diabetes in R6/2 mice [29]. More recently, we showed that intranasal administration of rhIGF-1 for 2 weeks, in order to promote IGF-1 delivery to the brain, enhanced IGF-1 cortical levels and improved motor activity and both peripheral and central metabolic abnormalities in YAC128 mice [30], an animal model presenting high levels of IGF-1 in plasma and expression in the striatum [26]. We also showed that rhIGF-1 intranasal administration in YAC128 mice activated Akt and increased mHtt phosphorylation at Ser421, suggesting that activation of IGF-1 signaling pathways is linked to amelioration of HD-associated glucose metabolic brain abnormalities and mice phenotype [30]. In lymphoblats from HD patients, we recently demonstrated that IGF-1 and insulin activate IR and IGF1R, Akt and Erk, and stimulate Htt phosphorylation at Ser421, increasing O_2 consumption, mitochondrial membrane potential, ATP and phosphocreatine levels, and decreasing lactate levels [84]. These data are consistent with stimulation of Akt signaling in insulin and IGF-1-treated HD cells.

Conversely to Akt, MEK/Erk1/2 was unchanged and both insulin and IGF-1 reduced Erk activation in mutant cells. Erk was previously described to protect against mHtt toxicity [85] and decreased p-Erk was found in ST*Hdh*$^{Q111/Q111}$ cells [86]. The difference obtained with the same cell model might be explained by the possibility that different ST*Hdh*$^{Q111/Q111}$ cell clones might have contrary results in some proteins [e.g. 47]. Previous data showed that IGF-1 may induce an early and transient Erk activation but abrogate the appearance of late and sustained Erk by activating PI-3K/protein kinase A, which phosphorylate c-Raf at Ser259, leading to Erk inhibition [87]. Also, insulin was shown to inhibit Erk1/2 phosphorylation in a PI-3K-dependent manner in Neuro2a cells [88]. In R6/2 HD mice, Fusco and collaborators [89] investigated Erk activation among different subsets of striatal neurons. They verified that the most susceptible striatal neurons to degeneration in HD, striatal medium spiny projection neurons and parvalbuminergic interneurons, exhibited increased p-Erk levels with disease progression. Conversely, the subsets of neurons that are more resistant to HD degeneration, namely somatostatin-NOS-NPY and cholinergic interneurons, showed decreased p-Erk with disease progression in the R6/2 mice [89]. This appears to indicate that Erk activity may be directly involved in HD progression and can define differences in striatal neuronal susceptibility.

Mitochondria in HD striatal cells were recently described to be altered and more vulnerable to oxidative stress [33,49]. Indeed, elevated mitochondrial $O_2^{\bullet-}$ generation in HD knock-in striatal cells has been linked to mitochondrial dysfunction [90,91]. In HD striatal neurons, ROS formation may be a consequence of mitochondrial dysfunction through defects of mitochondrial respiratory complexes [47], which occur early in disease progression, as recently shown by us [19]. Indeed, the striatum is highly susceptible to dysfunction of mitochondrial oxidative phosphorylation [92]. ROS formation in HD can further damage mitochondria by dissipating the mitochondrial membrane potential, dysregulating ATP production and leading to oxidation of mtDNA [8,23,93], which is highly vulnerable to oxidative damage due to its proximity to the respiratory chain, limited repair mechanisms, few non-coding sequences and lack of histones [94]. We have previously shown that $O_2^{\bullet-}$ formation also rises in HD human cybrids following exposure to 3-nitropropionic acid or staurosporine [43]. In this work, insulin and IGF-1 decreased mitochondrial $O_2^{\bullet-}$ formation in mutant cells. Concomitantly, insulin and IGF-1 improved mitochondrial function, evaluated through increased mitochondrial membrane potential, in a PI-3K/Akt-dependent manner in HD striatal cells. Enhanced mitochondrial function induced by the

peptides might be also related with reduced mitochondrial fragmentation in cells expressing mHtt. Indeed, we showed that insulin or IGF-1 treatment decreased p-Drp1/Drp1 levels. mHtt was previously described to bind Drp1, increasing its activity [62,63]. Increased Drp1 mRNA and protein levels were also found in the cortex and striatum of HD patients [9] in a grade-dependent manner [95]. We show here that MEK/Erk1/2 inhibition by U1026 greatly improved mitochondrial membrane potential, and enhanced IGF-1-induced increased mitochondrial membrane potential in mutant cells. Phosphorylated/active Erk was also increased in mitochondria of mutant cells. Recently, Erk was shown to phosphorylate and activate Drp1 resulting in increased mitochondrial fission [34], and to directly phosphorylate Tfam downregulating mitochondrial transcription [37].

It was previously described that Akt can accumulate in mitochondria in its active state [96], promoting increased expression and activity of complex I, inducing anaerobic glycolysis and mitochondrial respiration, directly phosphorylating α and β subunits of ATP synthase and thus increasing its activity [35] and evoking neuroprotection [36]. Importantly, treatment with insulin and IGF-1 increased mitochondrial p-(Thr308)Akt and total Akt levels in both striatal cells. Akt may phosphorylate HKII at Thr473, increasing HKII association with mitochondria [67], while Hsp60 directly interacts with Akt1 resulting in its activation [68]. Although IGF-1 significantly rose HKII levels in mitochondria of wild-type cells, mitochondrial Hsp60 levels were enhanced in both striatal cells, suggesting that IGF-1 might promote the refolding of stress-induced denatured proteins in mutant cells.

It was recently shown that mitochondrial protein import is inhibited by mHtt leading to neuronal death [97]. Here we show that mitochondrial levels of Tom20 and Tom40 are significantly enhanced by insulin in HD striatal cells, suggesting that the peptide may promote increased recognition, movement and import of cytosolically synthesized mitochondrial proteins. Tfam is required for mtDNA transcription and replication. In HD, polymorphisms in NRF-1 and Tfam were shown to be associated with age at onset in HD [98]. A reduction in Tfam levels in brain lysates from HD patients was previously found [95]. We showed decreased Tfam levels in HD lymphoblasts [84] and in mitochondria of mutant cells, suggesting that mHtt impairs mtDNA transcription and replication. Treatment with IGF-1, in particular, and insulin enhanced Tfam levels in mitochondria of mutant cells, underlying enhanced mtDNA transcription. Indeed, we detected increased levels of MT-COII in HD striatal cells upon treatment with IGF-1 and insulin.

The fact that insulin and IGF-1 might have mtDNA as a selective target in mutant cells *via* increased Tfam is consistent with the observation of unchanged NDUFS3, a nuclear-encoded subunit of complex I.

Although the role of Akt in mitochondria is not completely understood, active mitochondrial Akt has been shown to be neuroprotective [36]. Therefore, a better knowledge about the role of Akt in mitochondria of HD striatal cells might be essential to describe the role of insulin and IGF-1 on mitochondrial function.

In summary, our results show that insulin and IGF-1 (at low nM) activated cytosolic and mitochondrial Akt and inhibited Erk; this was accompanied by reduced p-Drp1/Drp1, suggesting reduced mitochondrial fission, and enhanced mitochondrial membrane potential in a process dependent on PI-3K/Akt signaling. Insulin and IGF-1 treatment further reduced mitochondrial ROS production and normalized mitochondrial SOD activity. Enhanced mitochondrial Tfam further underlay enhanced MT-COII levels in mitochondria of mutant cells, implicating increased function of the mitochondrial respiratory chain. Thus, insulin- and/or IGF-1-mediated intracellular PI3K/Akt signaling pathways may ameliorate mitochondrial function and ROS generation precluding apoptotic cell death in HD.

Acknowledgements

We wish to thank Doctor Luísa Cortes, head of MICC (Microscope Imaging Center of Coimbra) of CNC for the fluorescence microscopy image acquisition and analysis. This work was supported by European community fund_FEDER through "Programa Operacional Temático Factores de Competitividade – COMPETE" and "Fundação para a Ciência e a Tecnologia" (FCT), Portugal, project references PEst-C/SAU/LA0001/2013-2014, PTDC/SAU-FCF/66421/2006 and PTDC/SAU-FCF/108056/2008, M.R. PhD fellowship SFRH/BD/41285/2007 and T.R. postdoctoral fellowship SFRH/BPD/44246/2008.

References

[1] The Huntington's Disease Collaborative Research Group. A novel gene containing a trinucleotide repeat that is expanded and unstable on Huntington's disease chromosomes. *Cell* **72:**971-983; 1993.

[2] Gil, J. M.; Rego, A. C. Mechanisms of neurodegeneration in Huntington's disease. *Eur. J. Neurosci.* **27:**2803-2820; 2008.

[3] Rosenstock, T. R.; Duarte, A. I.; Rego, A. C. Mitochondrial-associated metabolic changes and neurodegeneration in Huntington's disease - from clinical features to the bench. *Curr. Drug Targets* **11:**1218-1236; 2010.

[4] Hersch, S. M.; Gevorkian, S.; Marder, K.; Moskowitz, C.; Feigin, A.; Cox, M.; Como, P.; Zimmerman, C.; Lin, M.; Zhang, L.; Ulug, A. M.; Beal, M. F.; Matson, W.; Bogdanov, M.; Ebbel, E.; Zaleta, A.; Kaneko, Y.; Jenkins, B.; Hevelone, N.; Zhang, H.; Yu, H.; Schoenfeld, D.; Ferrante, R.; Rosas, H. D. Creatine in Huntington disease is safe, tolerable, bioavailable in brain and reduces serum 8OH2'dG. *Neurology* **66:**250-252; 2006.

[5] Chen, C. M.; Wu, Y. R.; Cheng, M. L.; Liu, J. L.; Lee, Y. M.; Lee, P. W.; Soong, B. W.; Chiu, D. T. Increased oxidative damage and mitochondrial abnormalities in the peripheral blood of Huntington's disease patients. *Biochem. Biophys. Res. Commun.* **359:**335-340; 2007.

[6] Tunez, I.; Sanchez-Lopez, F.; Aguera, E.; Fernandez-Bolanos, R.; Sanchez, F. M.; Tasset-Cuevas, I. Important role of oxidative stress biomarkers in Huntington's disease. *J. Med. Chem.* **54:**5602-5606; 2011.

[7] Browne, S. E.; Bowling, A. C.; MacGarvey, U.; Baik, M. J.; Berger, S. C.; Muqit, M. M.; Bird, E. D.; Beal, M. F. Oxidative damage and metabolic dysfunction in Huntington's disease: selective vulnerability of the basal ganglia. *Ann. Neurol.* **41:**646-653; 1997.

[8] Polidori, M. C.; Mecocci, P.; Browne, S. E.; Senin, U.; Beal, M. F. Oxidative damage to mitochondrial DNA in Huntington's disease parietal cortex. *Neurosci. Lett.* **272:**53-56; 1999.

[9] Shirendeb, U.; Reddy, A. P.; Manczak, M.; Calkins, M. J.; Mao, P.; Tagle, D. A.; Reddy, P. H. Abnormal mitochondrial dynamics, mitochondrial loss and mutant huntingtin oligomers in Huntington's disease: implications for selective neuronal damage. *Hum. Mol. Genet.* **20:**1438-1455; 2011.

[10] Bogdanov, M. B.; Andreassen, O. A.; Dedeoglu, A.; Ferrante, R. J.; Beal, M. F. Increased oxidative damage to DNA in a transgenic mouse model of Huntington's disease. *J. Neurochem.* **79:**1246-1249; 2001.

[11] Stoy, N.; Mackay, G. M.; Forrest, C. M.; Christofides, J.; Egerton, M.; Stone, T. W.; Darlington, L. G. Tryptophan metabolism and oxidative stress in patients with Huntington's disease. *J. Neurochem.* **93:**611-623; 2005.

[12] Browne, S. E.; Ferrante, R. J.; Beal, M. F. Oxidative stress in Huntington's disease. *Brain Pathol.* **9:**147-163; 1999.

[13] Lee, J.; Kosaras, B.; Del Signore, S. J.; Cormier, K.; McKee, A.; Ratan, R. R.; Kowall, N. W.; Ryu, H. Modulation of lipid peroxidation and mitochondrial function improves neuropathology in Huntington's disease mice. *Acta Neuropathol.* **121:**487-498; 2011.

[14] Tabrizi, S. J.; Workman, J.; Hart, P. E.; Mangiarini, L.; Mahal, A.; Bates, G.; Cooper, J. M.; Schapira, A. H. Mitochondrial dysfunction and free radical damage in the Huntington R6/2 transgenic mouse. *Ann. Neurol.* **47:**80-86; 2000.

[15] Hands, S.; Sajjad, M. U.; Newton, M. J.; Wyttenbach, A. In vitro and in vivo aggregation of a fragment of huntingtin protein directly causes free radical production. *J. Biol. Chem.* **286:**44512-44520; 2011.

[16] Sorolla, M. A.; Reverter-Branchat, G.; Tamarit, J.; Ferrer, I.; Ros, J.; Cabiscol, E. Proteomic and oxidative stress analysis in human brain samples of Huntington disease. *Free Radic. Biol. Med.* **45:**667-678; 2008.

[17] Ribeiro, M.; Rosenstock, T. R.; Cunha-Oliveira, T.; Ferreira, I. L.; Oliveira, C. R.; Rego, A. C. Glutathione redox cycle dysregulation in Huntington's disease knock-in striatal cells. *Free Radic. Biol. Med.* **53:**1857-1867; 2012.

[18] Ehrlich, M. E. Huntington's disease and the striatal medium spiny neuron: cell-autonomous and non-cell-autonomous mechanisms of disease. *Neurotherapeutics* **9:**270-284; 2012.

[19] Silva, A. C.; Almeida, S.; Laco, M.; Duarte, A. I.; Domingues, J.; Oliveira, C. R.; Januario, C.; Rego, A. C. Mitochondrial respiratory chain complex activity and bioenergetic alterations in human platelets derived from pre-symptomatic and symptomatic Huntington's disease carriers. *Mitochondrion*; 2013.

[20] Napoli, E.; Wong, S.; Hung, C.; Ross-Inta, C.; Bomdica, P.; Giulivi, C. Defective mitochondrial disulfide relay system, altered mitochondrial morphology and function in Huntington's disease. *Hum. Mol. Genet.* **22:**989-1004; 2013.

[21] Panov, A. V.; Gutekunst, C. A.; Leavitt, B. R.; Hayden, M. R.; Burke, J. R.; Strittmatter, W. J.; Greenamyre, J. T. Early mitochondrial calcium defects in Huntington's disease are a direct effect of polyglutamines. *Nat. Neurosci.* **5:**731-736; 2002.

[22] Oliveira, J. M.; Chen, S.; Almeida, S.; Riley, R.; Goncalves, J.; Oliveira, C. R.; Hayden, M. R.; Nicholls, D. G.; Ellerby, L. M.; Rego, A. C. Mitochondrial-dependent Ca2+ handling in Huntington's disease striatal cells: effect of histone deacetylase inhibitors. *J. Neurosci.* **26:**11174-11186; 2006.

[23] Siddiqui, A.; Rivera-Sanchez, S.; Castro Mdel, R.; Acevedo-Torres, K.; Rane, A.; Torres-Ramos, C. A.; Nicholls, D. G.; Andersen, J. K.; Ayala-Torres, S. Mitochondrial DNA

damage is associated with reduced mitochondrial bioenergetics in Huntington's disease. *Free Radic. Biol. Med.* **53:**1478-1488; 2012.

[24] Xun, Z.; Rivera-Sanchez, S.; Ayala-Pena, S.; Lim, J.; Budworth, H.; Skoda, E. M.; Robbins, P. D.; Niedernhofer, L. J.; Wipf, P.; McMurray, C. T. Targeting of XJB-5-131 to mitochondria suppresses oxidative DNA damage and motor decline in a mouse model of Huntington's disease. *Cell Rep.* **2:**1137-1142; 2012.

[25] Choo, Y. S.; Johnson, G. V.; MacDonald, M.; Detloff, P. J.; Lesort, M. Mutant huntingtin directly increases susceptibility of mitochondria to the calcium-induced permeability transition and cytochrome c release. *Hum Mol Genet* **13:**1407-1420; 2004.

[26] Pouladi, M. A.; Xie, Y.; Skotte, N. H.; Ehrnhoefer, D. E.; Graham, R. K.; Kim, J. E.; Bissada, N.; Yang, X. W.; Paganetti, P.; Friedlander, R. M.; Leavitt, B. R.; Hayden, M. R. Full-length huntingtin levels modulate body weight by influencing insulin-like growth factor 1 expression. *Hum. Mol. Genet.* **19:**1528-1538; 2010.

[27] Humbert, S.; Bryson, E. A.; Cordelieres, F. P.; Connors, N. C.; Datta, S. R.; Finkbeiner, S.; Greenberg, M. E.; Saudou, F. The IGF-1/Akt pathway is neuroprotective in Huntington's disease and involves Huntingtin phosphorylation by Akt. *Dev. Cell* **2:**831-837; 2002.

[28] Gines, S.; Ivanova, E.; Seong, I. S.; Saura, C. A.; MacDonald, M. E. Enhanced Akt signaling is an early pro-survival response that reflects N-methyl-D-aspartate receptor activation in Huntington's disease knock-in striatal cells. *J. Biol. Chem.* **278:**50514-50522; 2003.

[29] Duarte, A. I.; Petit, G. H.; Ranganathan, S.; Li, J. Y.; Oliveira, C. R.; Brundin, P.; Bjorkqvist, M.; Rego, A. C. IGF-1 protects against diabetic features in an in vivo model of Huntington's disease. *Exp. Neurol.* **231:**314-319; 2011.

[30] Lopes, C.; Ribeiro, M.; Duarte, A. I.; Humbert, S.; Saudou, F.; de Almeida, L.P.; Hayden, M.; Rego, A.C. IGF-1 Intranasal Administration Rescues Huntington's Disease Phenotypes in YAC128 Mice. *Mol. Neurobiol.* in press; 2013.

[31] Duarte, A. I.; Santos, P.; Oliveira, C. R.; Santos, M. S.; Rego, A. C. Insulin neuroprotection against oxidative stress is mediated by Akt and GSK-3beta signaling pathways and changes in protein expression. *Biochim. Biophys. Acta* **1783:**994-1002; 2008.

[32] Langston, W.; Circu, M. L.; Aw, T. Y. Insulin stimulation of gamma-glutamylcysteine ligase catalytic subunit expression increases endothelial GSH during oxidative stress: influence of low glucose. *Free Radic. Biol. Med.* **45:**1591-1599; 2008.

[33] Jin, Y. N.; Yu, Y. V.; Gundemir, S.; Jo, C.; Cui, M.; Tieu, K.; Johnson, G. V. Impaired mitochondrial dynamics and Nrf2 signaling contribute to compromised responses to oxidative stress in striatal cells expressing full-length mutant huntingtin. *PLoS One* **8:**e57932; 2013.

[34] Gan, X.; Huang, S.; Wu, L.; Wang, Y.; Hu, G.; Li, G.; Zhang, H.; Yu, H.; Swerdlow, R. H.; Chen, J. X.; Yan, S. S. Inhibition of ERK-DLP1 signaling and mitochondrial division alleviates mitochondrial dysfunction in Alzheimer's disease cybrid cell. *Biochim Biophys Acta* **1842:**220-231; 2014.

[35] Li, C.; Li, Y.; He, L.; Agarwal, A. R.; Zeng, N.; Cadenas, E.; Stiles, B. L. PI3K/AKT signaling regulates bioenergetics in immortalized hepatocytes. *Free Radic. Biol. Med.* **60:**29-40; 2013.

[36] Mookherjee, P.; Quintanilla, R.; Roh, M. S.; Zmijewska, A. A.; Jope, R. S.; Johnson, G. V. Mitochondrial-targeted active Akt protects SH-SY5Y neuroblastoma cells from staurosporine-induced apoptotic cell death. *J Cell Biochem* **102:**196-210; 2007.

[37] Wang, K. Z.; Zhu, J.; Dagda, R. K.; Uechi, G.; Cherra, S. J., 3rd; Gusdon, A. M.; Balasubramani, M.; Chu, C. T. ERK-mediated phosphorylation of TFAM downregulates mitochondrial transcription: Implications for Parkinson's disease. *Mitochondrion*; 2014.

[38] Trettel, F.; Rigamonti, D.; Hilditch-Maguire, P.; Wheeler, V. C.; Sharp, A. H.; Persichetti, F.; Cattaneo, E.; MacDonald, M. E. Dominant phenotypes produced by the HD mutation in STHdh(Q111) striatal cells. *Hum. Mol. Genet.* **9:**2799-2809; 2000.

[39] LeBel, C. P.; Ischiropoulos, H.; Bondy, S. C. Evaluation of the probe 2',7'-dichlorofluorescin as an indicator of reactive oxygen species formation and oxidative stress. *Chem. Res. Toxicol.* **5:**227-231; 1992.

[40] Bindokas, V. P.; Jordan, J.; Lee, C. C.; Miller, R. J. Superoxide production in rat hippocampal neurons: selective imaging with hydroethidine. *J. Neurosci.* **16:**1324-1336; 1996.

[41] Filippi-Chiela, E. C.; Oliveira, M. M.; Jurkovski, B.; Callegari-Jacques, S. M.; da Silva, V. D.; Lenz, G. Nuclear morphometric analysis (NMA): screening of senescence, apoptosis and nuclear irregularities. *PLoS One* **7**:e42522; 2012.

[42] Nicholls, D. G. Fluorescence measurement of mitochondrial membrane potential changes in cultured cells. *Methods Mol. Biol.* **810:**119-133; 2012.

[43] Ferreira, I. L.; Nascimento, M. V.; Ribeiro, M.; Almeida, S.; Cardoso, S. M.; Grazina, M.; Pratas, J.; Santos, M. J.; Januario, C.; Oliveira, C. R.; Rego, A. C. Mitochondrial-dependent apoptosis in Huntington's disease human cybrids. *Exp. Neurol.* **222:**243-255; 2010.

[44] Rechler, M. M.; Zapf, J.; Nissley, S. P.; Froesch, E. R.; Moses, A. C.; Podskalny, J. M.; Schilling, E. E.; Humbel, R. E. Interactions of insulin-like growth factors I and II and multiplication-stimulating activity with receptors and serum carrier proteins. *Endocrinology* **107:**1451-1459; 1980.

[45] Robinson, K. M.; Janes, M. S.; Beckman, J. S. The selective detection of mitochondrial superoxide by live cell imaging. *Nat. Protoc.* **3:**941-947; 2008.

[46] Kalyanaraman, B.; Darley-Usmar, V.; Davies, K. J.; Dennery, P. A.; Forman, H. J.; Grisham, M. B.; Mann, G. E.; Moore, K.; Roberts, L. J., 2nd; Ischiropoulos, H. Measuring reactive oxygen and nitrogen species with fluorescent probes: challenges and limitations. *Free Radic. Biol. Med.* **52:**1-6; 2012.

[47] Lim, D.; Fedrizzi, L.; Tartari, M.; Zuccato, C.; Cattaneo, E.; Brini, M.; Carafoli, E. Calcium homeostasis and mitochondrial dysfunction in striatal neurons of Huntington disease. *J. Biol. Chem.* **283:**5780-5789; 2008.

[48] Rosenstock, T. R.; de Brito, O. M.; Lombardi, V.; Louros, S.; Ribeiro, M.; Almeida, S.; Ferreira, I. L.; Oliveira, C. R.; Rego, A. C. FK506 ameliorates cell death features in Huntington's disease striatal cell models. *Neurochem. Int.* **59:**600-609; 2011.

[49] Ribeiro, M.; Silva, A. C.; Rodrigues, J.; Naia, L.; Rego, A. C. Oxidizing effects of exogenous stressors in Huntington's disease knock-in striatal cells--protective effect of cystamine and creatine. *Toxicol Sci* **136:**487-499; 2013.

[50] Chen, Y.; Zhang, J.; Lin, Y.; Lei, Q.; Guan, K. L.; Zhao, S.; Xiong, Y. Tumour suppressor SIRT3 deacetylates and activates manganese superoxide dismutase to scavenge ROS. *EMBO Rep.* **12:**534-541; 2011.

[51] Nakaso, K.; Yano, H.; Fukuhara, Y.; Takeshima, T.; Wada-Isoe, K.; Nakashima, K. PI3K is a key molecule in the Nrf2-mediated regulation of antioxidative proteins by hemin in human neuroblastoma cells. *FEBS Lett* **546:**181-184; 2003.

[52] Moi, P.; Chan, K.; Asunis, I.; Cao, A.; Kan, Y. W. Isolation of NF-E2-related factor 2 (Nrf2), a NF-E2-like basic leucine zipper transcriptional activator that binds to the tandem

NF-E2/AP1 repeat of the beta-globin locus control region. *Proc. Natl. Acad. Sci. U.S.A.* **91:**9926-9930; 1994.

[53] Lau, A.; Tian, W.; Whitman, S. A.; Zhang, D. D. The predicted molecular weight of Nrf2: it is what it is not. *Antioxid. Redox Signal.* **18:**91-93; 2013.

[54] Huang, H. C.; Nguyen, T.; Pickett, C. B. Phosphorylation of Nrf2 at Ser-40 by protein kinase C regulates antioxidant response element-mediated transcription. *J Biol Chem* **277:**42769-42774; 2002.

[55] Fourquet, S.; Guerois, R.; Biard, D.; Toledano, M. B. Activation of NRF2 by nitrosative agents and H2O2 involves KEAP1 disulfide formation. *J Biol Chem* **285:**8463-8471; 2010.

[56] Vincent, E. E.; Elder, D. J.; Thomas, E. C.; Phillips, L.; Morgan, C.; Pawade, J.; Sohail, M.; May, M. T.; Hetzel, M. R.; Tavare, J. M. Akt phosphorylation on Thr308 but not on Ser473 correlates with Akt protein kinase activity in human non-small cell lung cancer. *Br. J. Cancer* **104:**1755-1761; 2011.

[57] Hahn-Windgassen, A.; Nogueira, V.; Chen, C. C.; Skeen, J. E.; Sonenberg, N.; Hay, N. Akt activates the mammalian target of rapamycin by regulating cellular ATP level and AMPK activity. *J. Biol. Chem.* **280:**32081-32089; 2005.

[58] Mayr, B.; Montminy, M. Transcriptional regulation by the phosphorylation-dependent factor CREB. *Nat Rev Mol. Cell. Biol.* **2:**599-609; 2001.

[59] Cui, L.; Jeong, H.; Borovecki, F.; Parkhurst, C. N.; Tanese, N.; Krainc, D. Transcriptional repression of PGC-1alpha by mutant huntingtin leads to mitochondrial dysfunction and neurodegeneration. *Cell* **127:**59-69; 2006.

[60] Cong, S. Y.; Pepers, B. A.; Evert, B. O.; Rubinsztein, D. C.; Roos, R. A.; van Ommen, G. J.; Dorsman, J. C. Mutant huntingtin represses CBP, but not p300, by binding and protein degradation. *Mol. Cell. Neurosci.* **30:**560-571; 2005.

[61] Steffan, J. S.; Kazantsev, A.; Spasic-Boskovic, O.; Greenwald, M.; Zhu, Y. Z.; Gohler, H.; Wanker, E. E.; Bates, G. P.; Housman, D. E.; Thompson, L. M. The Huntington's disease protein interacts with p53 and CREB-binding protein and represses transcription. *Proc. Natl. Acad. Sci. U.S.A.* **97:**6763-6768; 2000.

[62] Shirendeb, U. P.; Calkins, M. J.; Manczak, M.; Anekonda, V.; Dufour, B.; McBride, J. L.; Mao, P.; Reddy, P. H. Mutant huntingtin's interaction with mitochondrial protein Drp1 impairs mitochondrial biogenesis and causes defective axonal transport and synaptic degeneration in Huntington's disease. *Hum Mol Genet* **21:**406-420; 2012.

[63] Song, W.; Chen, J.; Petrilli, A.; Liot, G.; Klinglmayr, E.; Zhou, Y.; Poquiz, P.; Tjong, J.; Pouladi, M. A.; Hayden, M. R.; Masliah, E.; Ellisman, M.; Rouiller, I.; Schwarzenbacher, R.; Bossy, B.; Perkins, G.; Bossy-Wetzel, E. Mutant huntingtin binds the mitochondrial fission GTPase dynamin-related protein-1 and increases its enzymatic activity. *Nat Med* **17:**377-382; 2011.

[64] Cho, B.; Choi, S. Y.; Cho, H. M.; Kim, H. J.; Sun, W. Physiological and Pathological Significance of Dynamin-Related Protein 1 (Drp1)-Dependent Mitochondrial Fission in the Nervous System. *Exp Neurobiol* **22:**149-157; 2013.

[65] Vlahos, C. J.; Matter, W. F.; Hui, K. Y.; Brown, R. F. A specific inhibitor of phosphatidylinositol 3-kinase, 2-(4-morpholinyl)-8-phenyl-4H-1-benzopyran-4-one (LY294002). *J. Biol. Chem.* **269:**5241-5248; 1994.

[66] Namura, S.; Iihara, K.; Takami, S.; Nagata, I.; Kikuchi, H.; Matsushita, K.; Moskowitz, M. A.; Bonventre, J. V.; Alessandrini, A. Intravenous administration of MEK inhibitor U0126 affords brain protection against forebrain ischemia and focal cerebral ischemia. *Proc Natl Acad Sci U S A* **98:**11569-11574; 2001.

[67]Roberts, D. J.; Tan-Sah, V. P.; Smith, J. M.; Miyamoto, S. Akt phosphorylates HK-II at Thr-473 and increases mitochondrial HK-II association to protect cardiomyocytes. *J Biol Chem* **288:**23798-23806; 2013.

[68]Kapustian, L.; Kroupskaya, I.; Rozhko, O.; Bobyk, V.; Ryabenko, D.; Sidorik, L. Akt1 expression and activity at different stages in experimental heart failure. *Pathophysiology*; 2013.

[69]Piantadosi, C. A.; Suliman, H. B. Mitochondrial transcription factor A induction by redox activation of nuclear respiratory factor 1. *J Biol Chem* **281:**324-333; 2006.

[70] Santamaria, A.; Perez-Severiano, F.; Rodriguez-Martinez, E.; Maldonado, P. D.; Pedraza-Chaverri, J.; Rios, C.; Segovia, J. Comparative analysis of superoxide dismutase activity between acute pharmacological models and a transgenic mouse model of Huntington's disease. *Neurochem. Res.* **26:**419-424; 2001.

[71] van Roon-Mom, W. M.; Pepers, B. A.; t Hoen, P. A.; Verwijmeren, C. A.; den Dunnen, J. T.; Dorsman, J. C.; van Ommen, G. B. Mutant huntingtin activates Nrf2-responsive genes and impairs dopamine synthesis in a PC12 model of Huntington's disease. *BMC Mol. Biol.* **9:**84; 2008.

[72] Sun, Z.; Chin, Y. E.; Zhang, D. D. Acetylation of Nrf2 by p300/CBP augments promoter-specific DNA binding of Nrf2 during the antioxidant response. *Mol. Cell. Biol.* **29:**2658-2672; 2009.

[73] Gil, J.; Almeida, S.; Oliveira, C. R.; Rego, A. C. Cytosolic and mitochondrial ROS in staurosporine-induced retinal cell apoptosis. *Free Radic. Biol. Med.* **35:**1500-1514; 2003.

[74] Duarte, A. I.; Santos, M. S.; Oliveira, C. R.; Rego, A. C. Insulin neuroprotection against oxidative stress in cortical neurons--involvement of uric acid and glutathione antioxidant defenses. *Free Radic. Biol. Med.* **39:**876-889; 2005.

[75] Colin, E.; Regulier, E.; Perrin, V.; Durr, A.; Brice, A.; Aebischer, P.; Deglon, N.; Humbert, S.; Saudou, F. Akt is altered in an animal model of Huntington's disease and in patients. *Eur. J. Neurosci.* **21:**1478-1488; 2005.

[76] Maglione, V.; Marchi, P.; Di Pardo, A.; Lingrell, S.; Horkey, M.; Tidmarsh, E.; Sipione, S. Impaired ganglioside metabolism in Huntington's disease and neuroprotective role of GM1. *J. Neurosci.* **30:**4072-4080; 2010.

[77] Nagata, E.; Saiardi, A.; Tsukamoto, H.; Okada, Y.; Itoh, Y.; Satoh, T.; Itoh, J.; Margolis, R. L.; Takizawa, S.; Sawa, A.; Takagi, S. Inositol hexakisphosphate kinases induce cell death in Huntington disease. *J. Biol. Chem.* **286:**26680-26686; 2011.

[78] Zala, D.; Colin, E.; Rangone, H.; Liot, G.; Humbert, S.; Saudou, F. Phosphorylation of mutant huntingtin at S421 restores anterograde and retrograde transport in neurons. *Hum. Mol. Genet.* **17:**3837-3846; 2008.

[79] Warby, S. C.; Chan, E. Y.; Metzler, M.; Gan, L.; Singaraja, R. R.; Crocker, S. F.; Robertson, H. A.; Hayden, M. R. Huntingtin phosphorylation on serine 421 is significantly reduced in the striatum and by polyglutamine expansion in vivo. *Hum. Mol. Genet.* **14:**1569-1577; 2005.

[80] Sadagurski, M.; Cheng, Z.; Rozzo, A.; Palazzolo, I.; Kelley, G. R.; Dong, X.; Krainc, D.; White, M. F. IRS2 increases mitochondrial dysfunction and oxidative stress in a mouse model of Huntington disease. *J. Clin. Invest.* **121:**4070-4081; 2011.

[81] Yamamoto, A.; Cremona, M. L.; Rothman, J. E. Autophagy-mediated clearance of huntingtin aggregates triggered by the insulin-signaling pathway. *J. Cell. Biol.* **172:**719-731; 2006.

[82]Mochel, F.; Charles, P.; Seguin, F.; Barritault, J.; Coussieu, C.; Perin, L.; Le Bouc, Y.; Gervais, C.; Carcelain, G.; Vassault, A.; Feingold, J.; Rabier, D.; Durr, A. Early energy

deficit in Huntington disease: identification of a plasma biomarker traceable during disease progression. *PLoS One* **2:**e647; 2007.

[83] Saleh, N.; Moutereau, S.; Azulay, J. P.; Verny, C.; Simonin, C.; Tranchant, C.; El Hawajri, N.; Bachoud-Levi, A. C.; Maison, P.; Huntington French Speaking, G. High insulinlike growth factor I is associated with cognitive decline in Huntington disease. *Neurology* **75:**57-63; 2010.

[84] Naia, L.; Ferreira, I. L.; Cunha-Oliveira, T.; Duarte, A. I.; Ribeiro, M.; Rosenstock, T. R.; Laco, M. N.; Ribeiro, M. J.; Oliveira, C. R.; Saudou, F.; Humbert, S.; Rego, A. C. Activation of IGF-1 and Insulin Signaling Pathways Ameliorate Mitochondrial Function and Energy Metabolism in Huntington's Disease Human Lymphoblasts. *Mol Neurobiol*; 2014.

[85] Apostol, B. L.; Illes, K.; Pallos, J.; Bodai, L.; Wu, J.; Strand, A.; Schweitzer, E. S.; Olson, J. M.; Kazantsev, A.; Marsh, J. L.; Thompson, L. M. Mutant huntingtin alters MAPK signaling pathways in PC12 and striatal cells: ERK1/2 protects against mutant huntingtin-associated toxicity. *Hum. Mol. Genet.* **15:**273-285; 2006.

[86] Sarantos, M. R.; Papanikolaou, T.; Ellerby, L. M.; Hughes, R. E. Pizotifen Activates ERK and Provides Neuroprotection in vitro and in vivo in Models of Huntington's Disease. *J. Huntingtons Dis.* **1:**195-210; 2012.

[87] Subramaniam, S.; Shahani, N.; Strelau, J.; Laliberte, C.; Brandt, R.; Kaplan, D.; Unsicker, K. Insulin-like growth factor 1 inhibits extracellular signal-regulated kinase to promote neuronal survival via the phosphatidylinositol 3-kinase/protein kinase A/c-Raf pathway. *J Neurosci* **25:**2838-2852; 2005.

[88] van der Heide, L. P.; Hoekman, M. F.; Biessels, G. J.; Gispen, W. H. Insulin inhibits extracellular regulated kinase 1/2 phosphorylation in a phosphatidylinositol 3-kinase (PI3) kinase-dependent manner in Neuro2a cells. *J Neurochem* **86:**86-91; 2003.

[89] Fusco, F. R.; Anzilotti, S.; Giampa, C.; Dato, C.; Laurenti, D.; Leuti, A.; Colucci D'Amato, L.; Perrone, L.; Bernardi, G.; Melone, M. A. Changes in the expression of extracellular regulated kinase (ERK 1/2) in the R6/2 mouse model of Huntington's disease after phosphodiesterase IV inhibition. *Neurobiol. Dis.* **46:**225-233; 2012.

[90] Milakovic, T.; Johnson, G. V. Mitochondrial respiration and ATP production are significantly impaired in striatal cells expressing mutant huntingtin. *J. Biol. Chem.* **280:**30773-30782; 2005.

[91] Quintanilla, R. A.; Jin, Y. N.; Fuenzalida, K.; Bronfman, M.; Johnson, G. V. Rosiglitazone treatment prevents mitochondrial dysfunction in mutant huntingtin-expressing cells: possible role of peroxisome proliferator-activated receptor-gamma (PPARgamma) in the pathogenesis of Huntington disease. *J. Biol. Chem.* **283:**25628-25637; 2008.

[92] Pickrell, A. M.; Fukui, H.; Wang, X.; Pinto, M.; Moraes, C. T. The striatum is highly susceptible to mitochondrial oxidative phosphorylation dysfunctions. *J. Neurosci.* **31:**9895-9904; 2011.

[93] Acevedo-Torres, K.; Berrios, L.; Rosario, N.; Dufault, V.; Skatchkov, S.; Eaton, M. J.; Torres-Ramos, C. A.; Ayala-Torres, S. Mitochondrial DNA damage is a hallmark of chemically induced and the R6/2 transgenic model of Huntington's disease. *DNA Repair (Amst.)* **8:**126-136; 2009.

[94] Richter, C.; Park, J. W.; Ames, B. N. Normal oxidative damage to mitochondrial and nuclear DNA is extensive. *Proc. Natl. Acad. Sci. U.S.A.* **85:**6465-6467; 1988.

[95]Kim, J.; Moody, J. P.; Edgerly, C. K.; Bordiuk, O. L.; Cormier, K.; Smith, K.; Beal, M. F.; Ferrante, R. J. Mitochondrial loss, dysfunction and altered dynamics in Huntington's disease. *Hum Mol Genet* **19:**3919-3935; 2010.

[96] Bijur, G. N.; Jope, R. S. Rapid accumulation of Akt in mitochondria following phosphatidylinositol 3-kinase activation. *J. Neurochem.* **87:**1427-1435; 2003.

[97] Yano, H.; Baranov, S. V.; Baranova, O. V.; Kim, J.; Pan, Y.; Yablonska, S.; Carlisle, D. L.; Ferrante, R. J.; Kim, A. H.; Friedlander, R. M. Inhibition of mitochondrial protein import by mutant huntingtin. *Nat Neurosci* **17:**822-831; 2014.

[98] Taherzadeh-Fard, E.; Saft, C.; Akkad, D. A.; Wieczorek, S.; Haghikia, A.; Chan, A.; Epplen, J. T.; Arning, L. PGC-1alpha downstream transcription factors NRF-1 and TFAM are genetic modifiers of Huntington disease. *Mol Neurodegener* **6:**32; 2011.

Figure legends

Figure 1. Insulin and IGF-1 protect from mitochondrial ROS formation in HD striatal cells. Mitochondrial superoxide anion ($O_2^{\bullet-}$) formation measured with (**A**) MitoSOX Red and (**B**) DHE in wild-type and mutant striatal cells. (**A**) Cells were exposed to insulin or IGF-1 (0.1 nM) during 24 h. (**B**) Intracellular $O_2^{\bullet-}$ formation was further analysed following exposure to mitochondrial complex I (rotenone) and III (antimycin A) inhibitors (10 μM, for 1h). Data are the mean ± S.E.M. of 3-6 independent experiments. Statistical analysis: $^{+++}P<0.0001$ when comparing mutant *versus* wild-type cells by Student's *t*-test; $^{***}P<0.0001$ by two-way ANOVA for multiple groups using Bonferroni as post-hoc test, when comparing mutant *versus* wild-type cells; or $^{\#\#}P<0.01$ and $^{\#\#\#}P<0.0001$ by two-way ANOVA when comparing treated *versus* non-treated (control) cells.

Figure 2. Insulin and IGF-1 protect from caspase-3 activation and nuclear irregularities in HD striatal cells. (**A**) Caspase-3 activity in wild-type and mutant cells was tested following exposure to insulin or IGF-1 (0.1 nM) during 24h. Apoptotic or senescent nuclei was also analysed in (**B**) wild-type or (**C**) mutant striatal cells following incubation with insulin or IGF-1 (0.1 nM) during 24h. Data are the mean ± S.E.M. of 4 independent experiments. Statistical

analysis: $^{**}P<0.01$ and $^{***}P<0.0001$ by two-way ANOVA for multiple groups using Bonferroni as post-hoc test, when comparing mutant *versus* wild-type cells; $^{\#}P<0.05$, $^{\#\#}P<0.01$ and $^{\#\#\#}P<0.0001$ by two-way ANOVA when comparing treated *versus* non-treated (control) cells, $^{\S}P<0.05$, $^{\S\S}P<0.01$ and $^{\S\S\S}P<0.0001$ by one-way ANOVA using Bonferroni as post-hoc test when comparing normal treated nuclei versus apoptotic or senescent treated nuclei.

Figure 3. Insulin and IGF-1 restored mitochondrial SOD activity in HD striatal cells. (**A**) Total and (**B**) mitochondrial SOD2 (Mn-SOD) activities in wild-type and mutant striatal cells. (**C**) Ac(Lys68)SOD2/SOD2 ratio and (**D**) SOD2 protein levels were measured after incubation with insulin or IGF-1 (0.1 nM, for 24 h). (**E**) Total and (**F**) mitochondrial SOD1 (Cu/Zn-SOD) activities and (**G**) SOD1 protein levels were measured in wild-type and mutant cells. In (**H**) mitochondrial SOD1/2 activity was analysed in striatal cells subjected to insulin or IGF-1 (0.1 nM, for 24 h). Data are the mean ± S.E.M. of 3-4 independent experiments. Statistical analysis: $^{+++}P<0.0001$ by Student's *t*-test comparing mutant *versus* wild-type cells; $^{t}P<0.05$ by Student's *t*-test comparing treated *versus* non-treated conditions; $^{*}P<0.05$, $^{**}P<0.01$ and $^{***}P<0.0001$ by two-way ANOVA when comparing mutant *versus* wild-type cells; $^{\#\#}P<0.01$ and $^{\#\#\#}P<0.0001$ by two-way ANOVA when comparing treated *versus* non-treated (control) cells.

Figure 4. Insulin increases GCLc protein levels in mutant cells. (**A**,**B**) GCLc protein levels in wild-type and mutant striatal cells exposed to 0.1 and 1 nM (**A**) insulin or (**B**) IGF-1 (24h-treatment). (**C**) GSH and (**D**) GSSG levels were analysed in both striatal cells after exposure to insulin or IGF-1 (0.1 nM). Data are the mean ± S.E.M. of 4 independent experiments. Statistical analysis: $^{*}P<0.05$, $^{**}P<0.01$ and $^{***}P<0.0001$ by two-way ANOVA when comparing mutant *versus* wild-type cells; $^{\#}P<0.05$ and $^{\#\#}P<0.01$ by two-way ANOVA when comparing treated *versus* non-treated (control) cells.

Figure 5. Insulin and IGF-1 increase nuclear levels of phosphorylated Nrf2 in mutant cells. Striatal cells were treated with 0.1 nM insulin or IGF-1 during 24 h or 500 µM H_2O_2 during 3 h for determination of cellular (**A,B**) p-(Ser40)Nrf2/Nrf2 and nuclear (**C,D**) p-(Ser40)Nrf2/Nrf2 levels and (**E**) Nrf2/ARE transcriptional activity by the luciferase reporter assay. Representative blots for (**B**) cellular p-Nrf2, Nrf2 and actin, or (**D**) nuclear p-Nrf2, Nrf2 and TBP. Results are the

mean ± S.E.M. of 3-7 independent experiments. Statistical analysis: $^{+++}P<0.0001$ by Student's *t*-test comparing mutant *versus* wild-type cells; $^{t}P<0.05$ and $^{tt}P<0.01$ by Student's *t*-test comparing treated *versus* non-treated conditions. $^{***}P<0.0001$ by two-way ANOVA when comparing mutant *versus* wild-type cells; $^{\#}P<0.05$ and $^{\#\#}P<0.01$ by two-way ANOVA when comparing treated *versus* non-treated (control) cells.

Figure 6. Insulin and IGF-1 promote Akt activation and Erk inhibition in HD striatal cells. Wild-type and mutant striatal cells were treated with 0.1 nM insulin or IGF-1 during 24 h for determination of cytosolic (**A,C**) p-(Thr308)Akt/Akt, (**B,C**) Akt/actin, and cellular (**D,F**) p-(Thr202/Tyr204)Erk1/2, and (**E,F**) Erk/actin ratio. Representative blots for (**C**) p-(Thr308)Akt, Akt, and actin, and (**F**) p-(Thr202/Tyr204)Erk1/2, Erk1/2 and actin. Data are the mean ± S.E.M. of 3-4 independent experiments. Statistical analysis: $^{+}P<0.05$ and $^{++}P<0.01$ by Student's *t*-test comparing mutant *versus* wild-type cells; $^{t}P<0.05$ and $^{ttt}P<0.0001$ by Student's *t*-test comparing treated *versus* non-treated conditions. $^{**}P<0.01$ by two-way ANOVA when comparing mutant *versus* wild-type cells; $^{\#}P<0.05$, $^{\#\#}P<0.01$ and $^{\#\#\#}P<0.0001$ by two-way ANOVA when comparing treated *versus* non-treated (control) cells.

Figure 7. Insulin, IGF-1 and U126 increase mitochondrial membrane potential in HD striatal cells. (**A-E**) Wild-type and mutant striatal cells were treated with 0.1 nM insulin or IGF-1, during 24h, for determination of mitochondrial levels of (**A**,**C**) p-(Ser616)Drp1/Drp1 and (**B**,**C**) Drp1, and (**D-I**) mitochondrial membrane potential using $TMRM^{+}$. (**C**) Representative blots of mitochondrial fractions labelled for pDrp1, Drp1, SDHA (used to normalize data for mitochondrial proteins), and Nrf2 (used as a cytosolic and nuclear protein to verify the purity of mitochondrial fractions). In **E** the cells were exposed to 500 μM H_2O_2 during 3 h. Wild-type (**F,H**) or mutant (**G,I**) striatal cells were also incubated in the absence or presence of 25 μM LY294002, a PI-3K/Akt inhibitor (**F,G**) or 10 μM U0126, an inhibitor of MEK/Erk activity (**H,I**) during 24 h. Data are the mean ± S.E.M. of 4-8 independent experiments. Statistical analysis: $^{+++}P<0.0001$ by Student's *t*-test comparing mutant *versus* wild-type cells; $^{t}P<0.05$ by Student's *t*-test comparing treated *versus* non-treated conditions; $^{*}P<0.05$ and $^{***}P<0.0001$ by two-way ANOVA when comparing mutant *versus* wild-type cells; $^{\#}P<0.05$ and $^{\#\#\#}P<0.0001$ by two-way ANOVA when comparing treated *versus* non-treated (control) cells. $^{@}P<0.05$ and $^{@@@}P<0.0001$

by one-way ANOVA when comparing treated *versus* non-treated (control) cells. $^{\S}P<0.05$ and $^{\S\S\S}P<0.0001$ by one-way ANOVA when comparing insulin or IGF-1 *versus* LY294002 plus insulin or IGF-1 or insulin or IGF-1 *versus* U0126 plus insulin or IGF-1 treatment in both striatal cells.

Figure 8. Insulin and IGF-1 enhance the levels of mitochondrial proteins involved in signaling, protein import and folding, mtDNA transcription and bioenergetics in HD striatal cells. Wild-type and mutant striatal cells were treated with 0.1 nM insulin or IGF-1, during 24 h, for analysis of several proteins in mitochondrial fractions, namely (**A,L**) p-(Thr308)Akt, (**B,L**) Akt, (**C**,**L**) p-(Thr202/Tyr204)Erk1/2, (**D**,**L**) Erk1/2, (**E**,**L**) hexokinase type II (HKII), (**F**,**L**) heat shock 60kDa protein 1 (Hsp60), (**G**,**L**) translocase of outer mitochondrial membrane 20 homolog (yeast) (Tom20), (**H**,**L**) translocase of outer mitochondrial membrane 40 homolog (yeast) (Tom40), (**I**,**L**) transcription factor A, mitochondrial (Tfam), (**J**,**L**) NADH dehydrogenase (ubiquinone) Fe-S protein 3, 30kDa (NADH-coenzyme Q reductase) (NDUFS3) and (**K**,**L**) mitochondrial-encoded cytochrome c oxidase II (MT-COII). (**L**) Representative blots of proteins depicted in **A-K,** in which succinate dehydrogenase complex, subunit A, flavoprotein (Fp) (SDHA) was used to normalize data of other mitochondrial proteins; Nrf2 was used as a cytosolic and nuclear protein to verify the purity of mitochondrial fractions. Data are the mean ± S.E.M. of 4 independent experiments. Statistical analysis: $^{++}P<0.01$ and $^{+++}P<0.0001$ by Student's *t*-test comparing mutant *versus* wild-type cells; $^{t}P<0.05$, $^{tt}P<0.01$, and $^{ttt}P<0.0001$ by Student's *t*-test comparing treated *versus* non-treated conditions; $^{*}P<0.05$, $^{**}P<0.01$ and $^{***}P<0.0001$ by two-way ANOVA when comparing mutant *versus* wild-type cells; $^{\#}P<0.05$, $^{\#\#}P<0.01$ and $^{\#\#\#}P<0.0001$ by two-way ANOVA when comparing treated *versus* non-treated (control) cells.

Highlights:

- Insulin/IGF-1 precludes mHtt-induced mitochondrial ROS formation and SOD activity.
- Insulin/IGF-1 protection in HD cells is independent of Nrf2 transcription activity.
- Insulin/IGF-1 enhances mitochondrial function via PI3K/Akt pathway in HD cells.
- Insulin/IGF-1 increases p-Akt, Tfam and MT-COII in mitochondria of HD cells.

Figures 1-8

Fig. 1

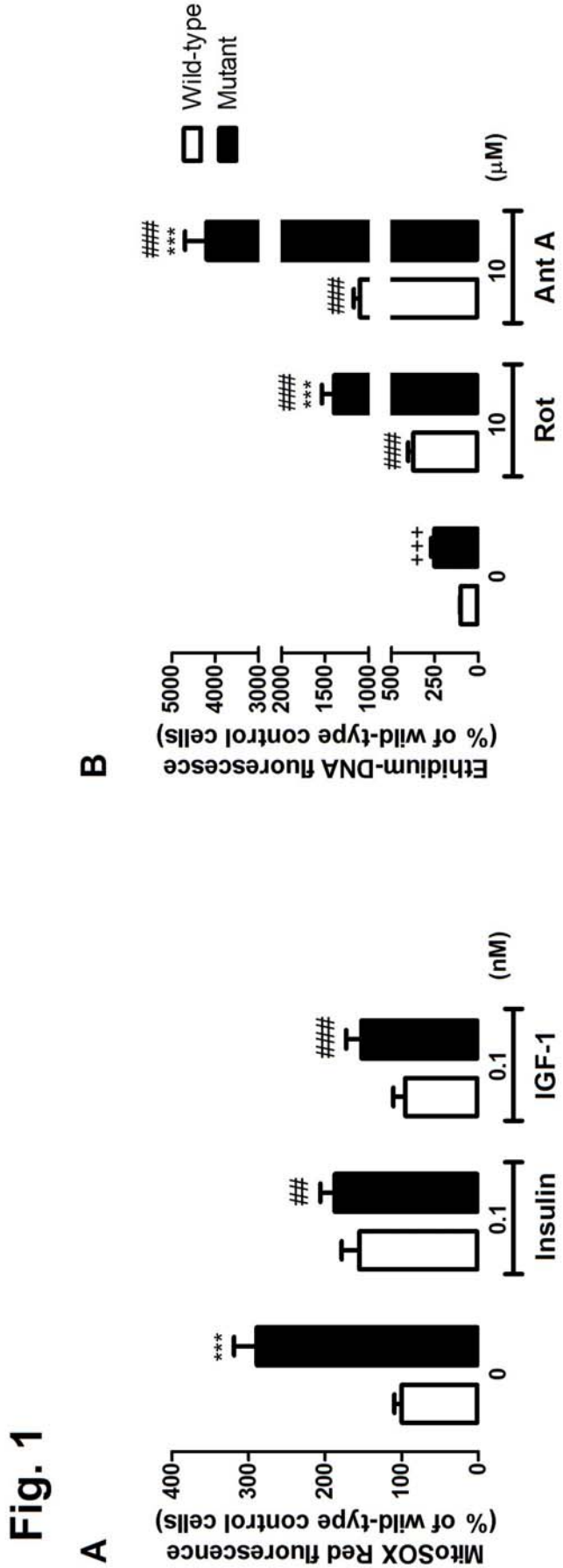

Fig. 2

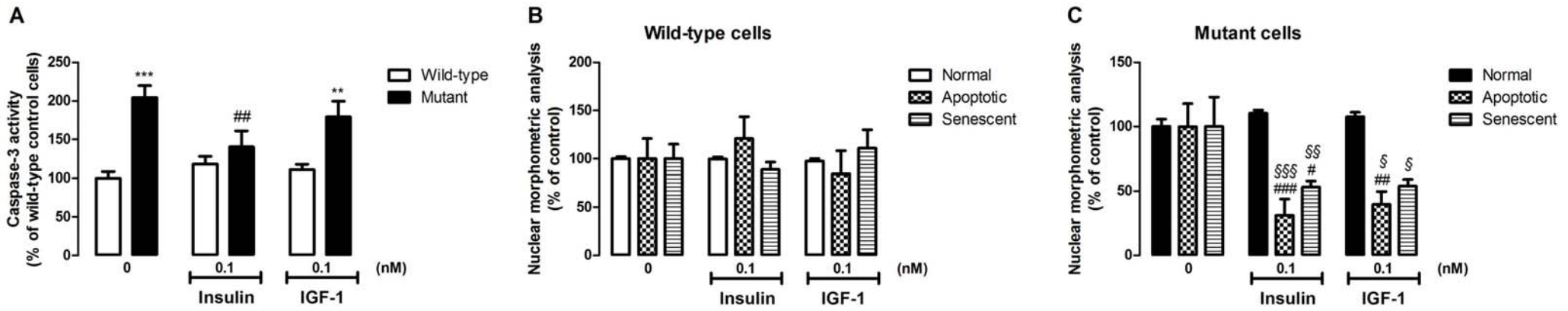

Fig. 3

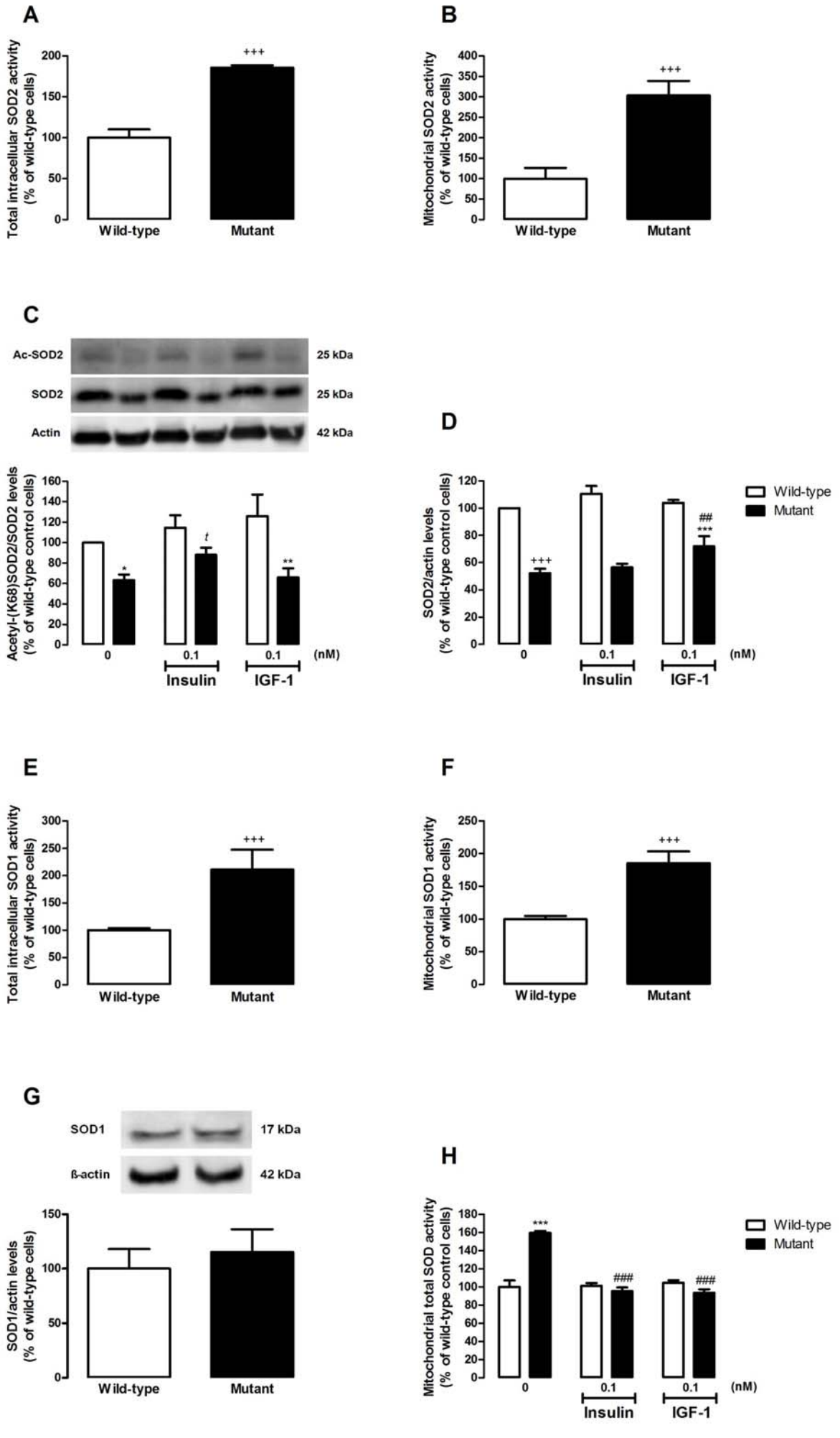
A
Total intracellular SOD2 activity (% of wild-type cells)
200
150
100
50
0
+++
Wild-type
Mutant
B
Mitochondrial SOD2 activity (% of wild-type cells)
400
350
300
250
200
150
100
50
0
+++
Wild-type
Mutant
C
Ac-SOD2
SOD2
Actin
25 kDa
25 kDa
42 kDa
Acetyl-(K68)SOD2/SOD2 levels (% of wild-type control cells)
160
140
120
100
80
60
40
20
0
*
t
**
0
0.1
0.1
(nM)
Insulin
IGF-1
D
SOD2/actin levels (% of wild-type control cells)
120
100
80
60
40
20
0
+++
##
***
Wild-type
Mutant
0
0.1
0.1
(nM)
Insulin
IGF-1
E
Total intracellular SOD1 activity (% of wild-type cells)
300
250
200
150
100
50
0
+++
Wild-type
Mutant
F
Mitochondrial SOD1 activity (% of wild-type cells)
250
200
150
100
50
0
+++
Wild-type
Mutant
G
SOD1
ß-actin
17 kDa
42 kDa
SOD1/actin levels (% of wild-type cells)
150
100
50
0
Wild-type
Mutant
H
Mitochondrial total SOD activity (% of wild-type control cells)
180
160
140
120
100
80
60
40
20
0
***
###
###
Wild-type
Mutant
0
0.1
0.1
(nM)
Insulin
IGF-1

Fig. 4

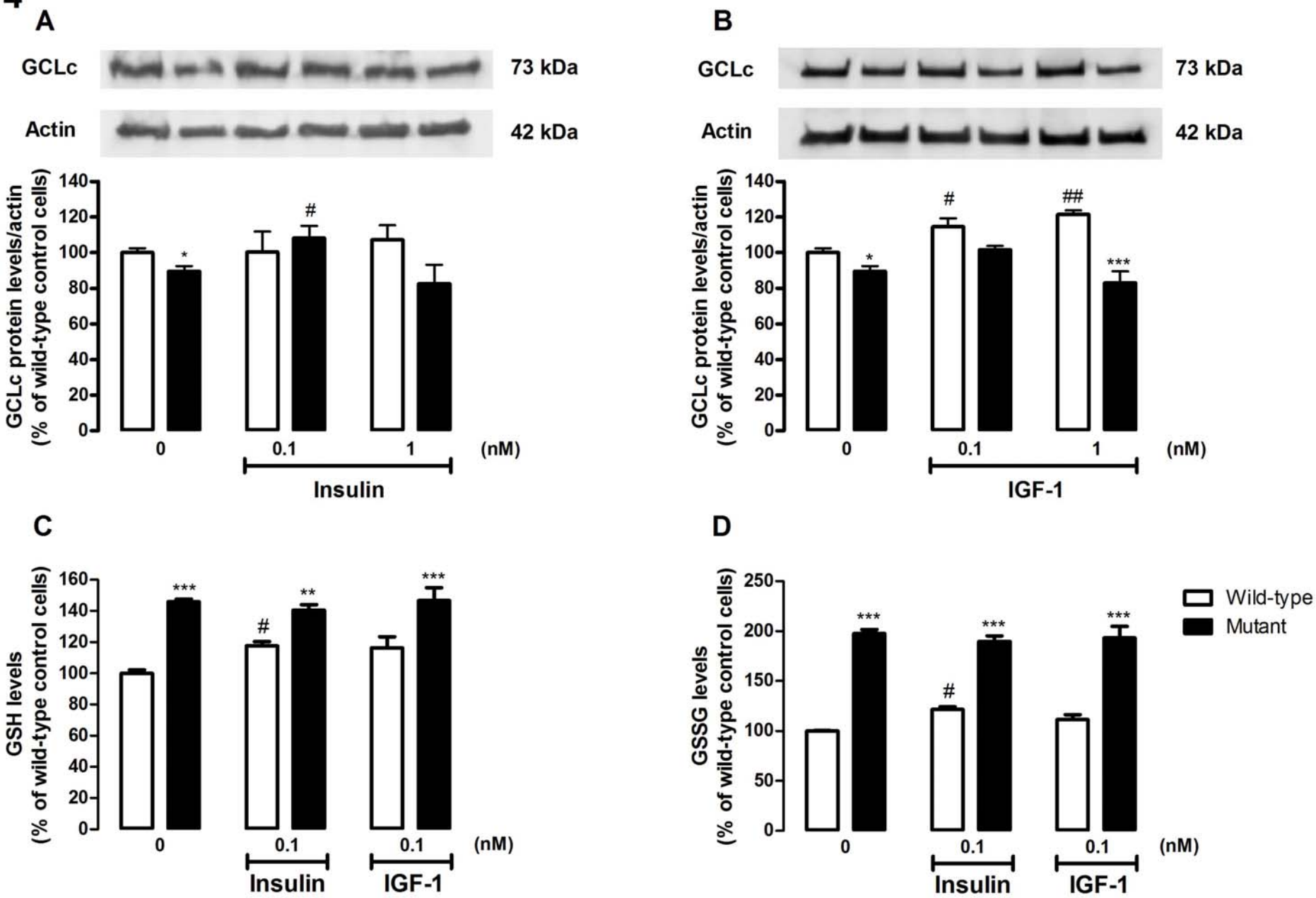

Fig. 5

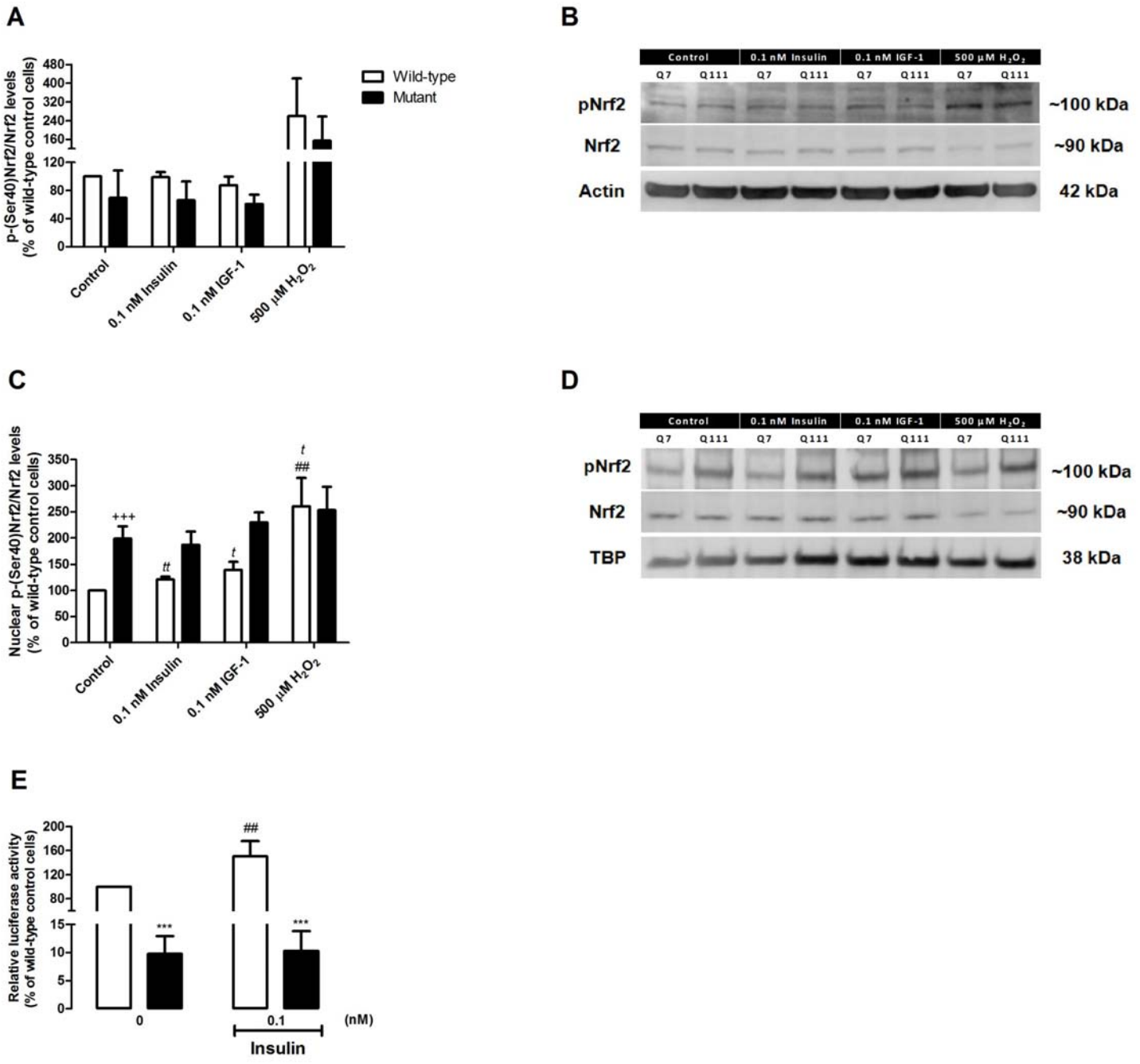

Fig. 6

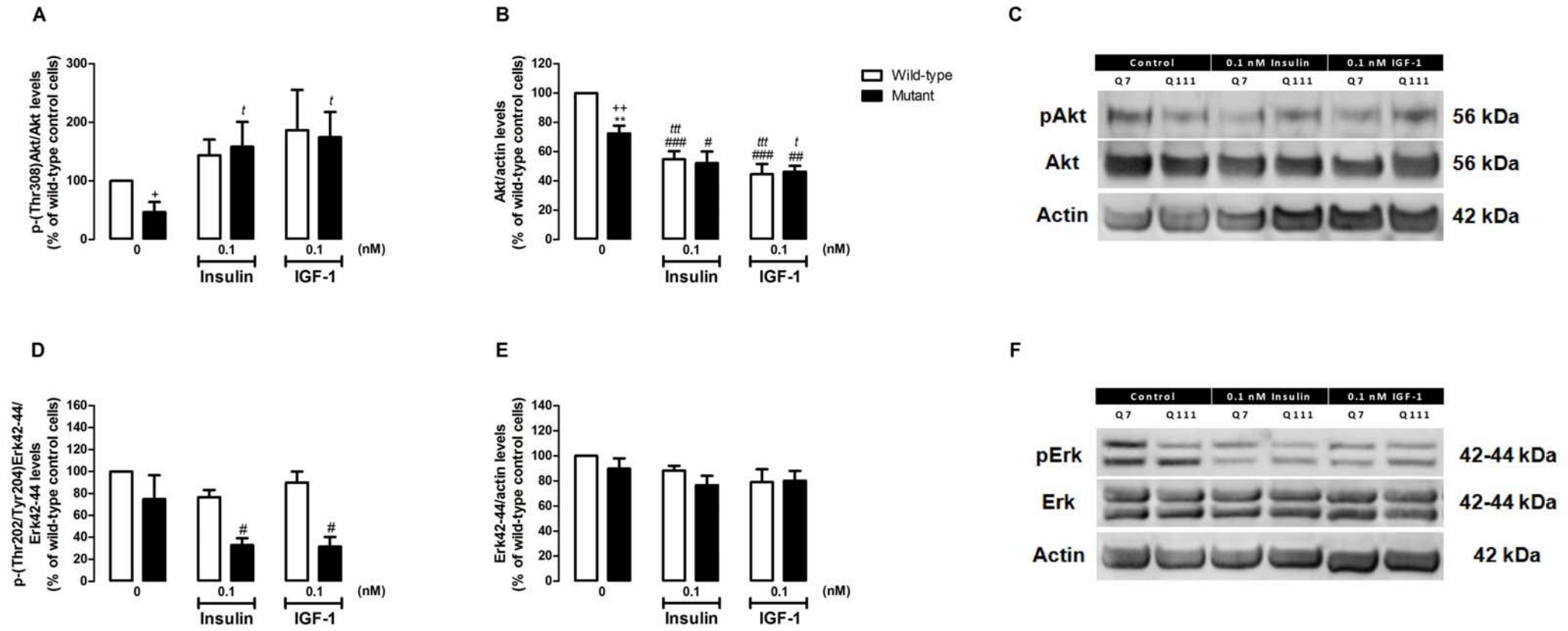
A
p-(Thr308)Akt/Akt levels
(% of wild-type control cells)
300
200
100
0
+
t
t
0
0.1
0.1
(nM)
Insulin
IGF-1
B
Akt/actin levels
(% of wild-type control cells)
120
100
80
60
40
20
0
++
**
ttt
###
#
ttt
###
t
##
Wild-type
Mutant
0
0.1
0.1
(nM)
Insulin
IGF-1
C
Control
0.1 nM Insulin
0.1 nM IGF-1
Q7
Q111
Q7
Q111
Q7
Q111
pAkt
56 kDa
Akt
56 kDa
Actin
42 kDa
D
p-(Thr202/Tyr204)Erk42-44/
Erk42-44 levels
(% of wild-type control cells)
160
140
120
100
80
60
40
20
0
#
#
0
0.1
0.1
(nM)
Insulin
IGF-1
E
Erk42-44/actin levels
(% of wild-type control cells)
140
120
100
80
60
40
20
0
0
0.1
0.1
(nM)
Insulin
IGF-1
F
Control
0.1 nM Insulin
0.1 nM IGF-1
Q7
Q111
Q7
Q111
Q7
Q111
pErk
42-44 kDa
Erk
42-44 kDa
Actin
42 kDa

Fig. 7

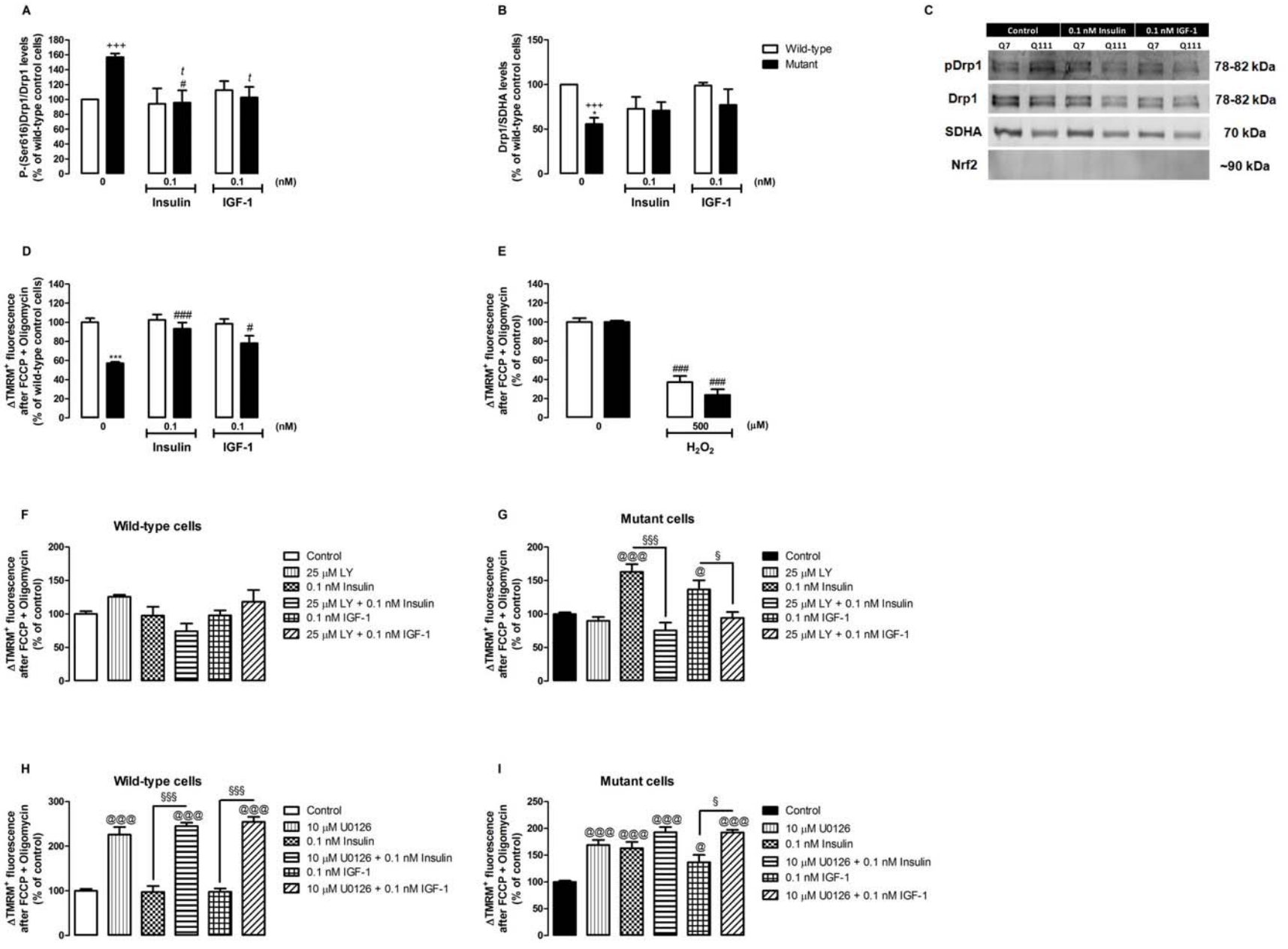

Fig. 8

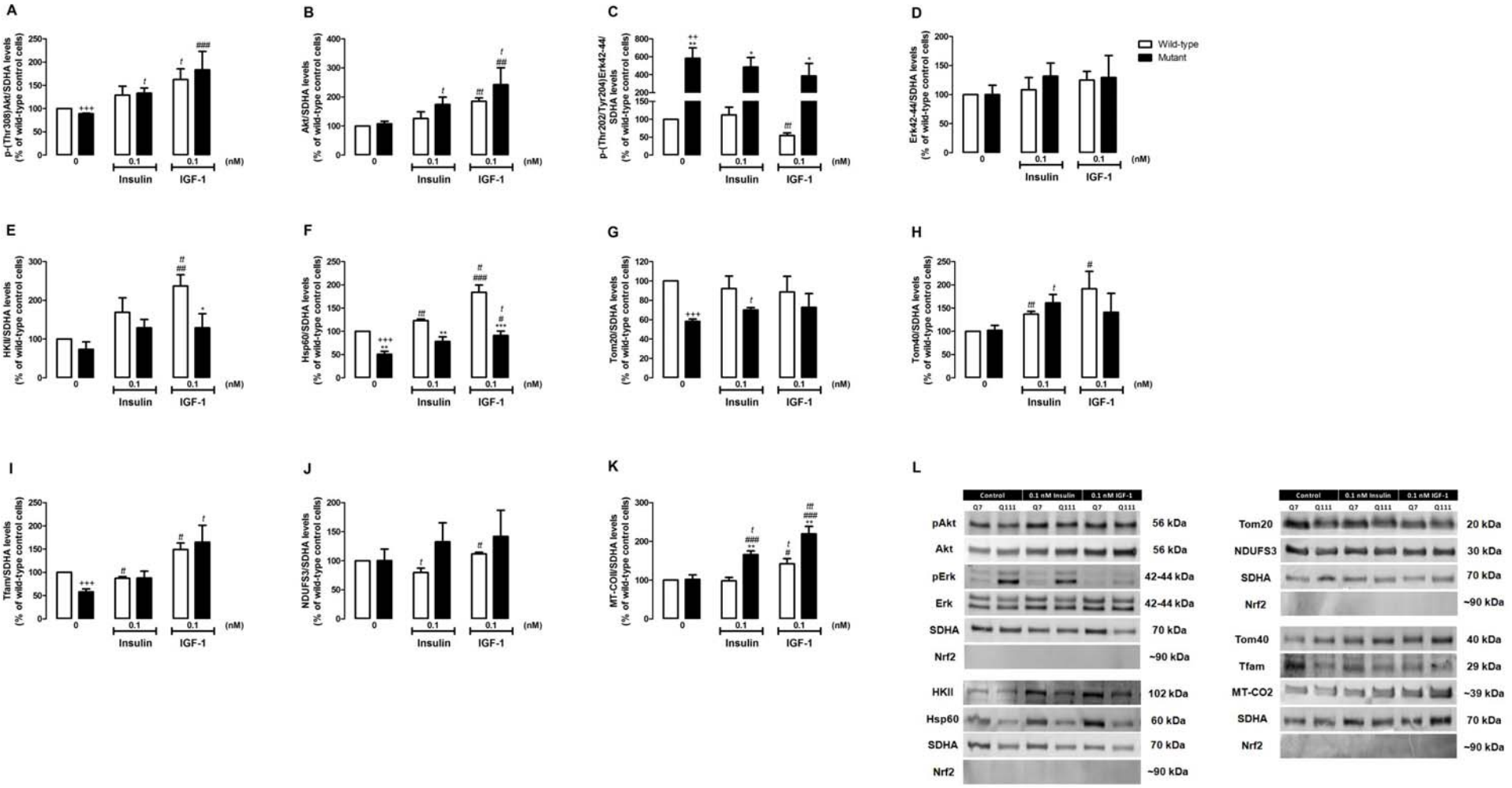
A
p-(Thr308)Akt/SDHA levels (% of wild-type control cells)
B
Akt/SDHA levels (% of wild-type control cells)
C
p-(Thr202/Tyr204)Erk42-44/ SDHA levels (% of wild-type control cells)
D
Erk42-44/SDHA levels (% of wild-type control cells)
Wild-type
Mutant
E
HKII/SDHA levels (% of wild-type control cells)
F
Hsp60/SDHA levels (% of wild-type control cells)
G
Tom20/SDHA levels (% of wild-type control cells)
H
Tom40/SDHA levels (% of wild-type control cells)
I
Tfam/SDHA levels (% of wild-type control cells)
J
NDUFS3/SDHA levels (% of wild-type control cells)
K
MT-COII/SDHA levels (% of wild-type control cells)
0
0.1
0.1
(nM)
Insulin
IGF-1

L
Control
0.1 nM Insulin
0.1 nM IGF-1
Q7
Q111
pAkt
Akt
pErk
Erk
SDHA
Nrf2
HKII
Hsp60
56 kDa
56 kDa
42-44 kDa
42-44 kDa
70 kDa
~90 kDa
102 kDa
60 kDa
70 kDa
~90 kDa
Tom20
NDUFS3
SDHA
Nrf2
Tom40
Tfam
MT-CO2
SDHA
Nrf2
20 kDa
30 kDa
70 kDa
~90 kDa
40 kDa
29 kDa
~39 kDa
70 kDa
~90 kDa

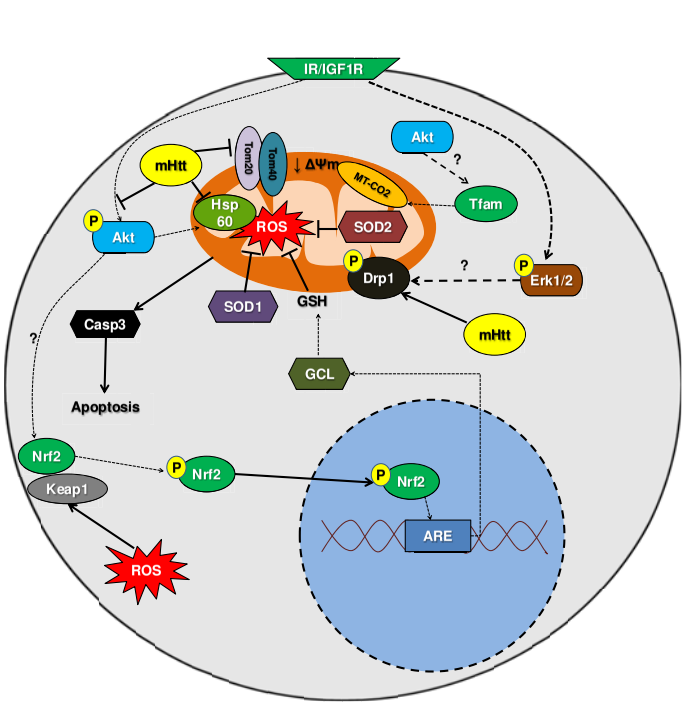
IR/IGF1R
mHtt
Tom20
Tom40
↓ ΔΨm
MT-CO2
Akt
Tfam
Hsp 60
ROS
SOD2
P
Akt
SOD1
GSH
Drp1
Erk1/2
Casp3
mHtt
GCL
Apoptosis
Nrf2
Keap1
Nrf2
Nrf2
ARE
ROS

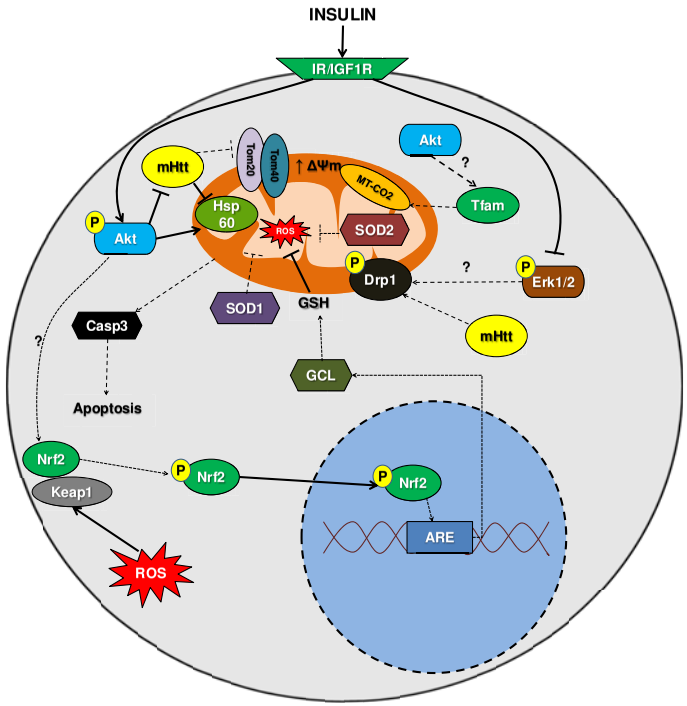
INSULIN
IR/IGF1R
mHtt
Tom20
Tom40
↑ ΔΨm
MT-CO2
Akt
Tfam
Hsp 60
ROS
SOD2
P
Akt
SOD1
GSH
Drp1
Erk1/2
Casp3
mHtt
GCL
Apoptosis
Nrf2
Keap1
Nrf2
Nrf2
ARE
ROS

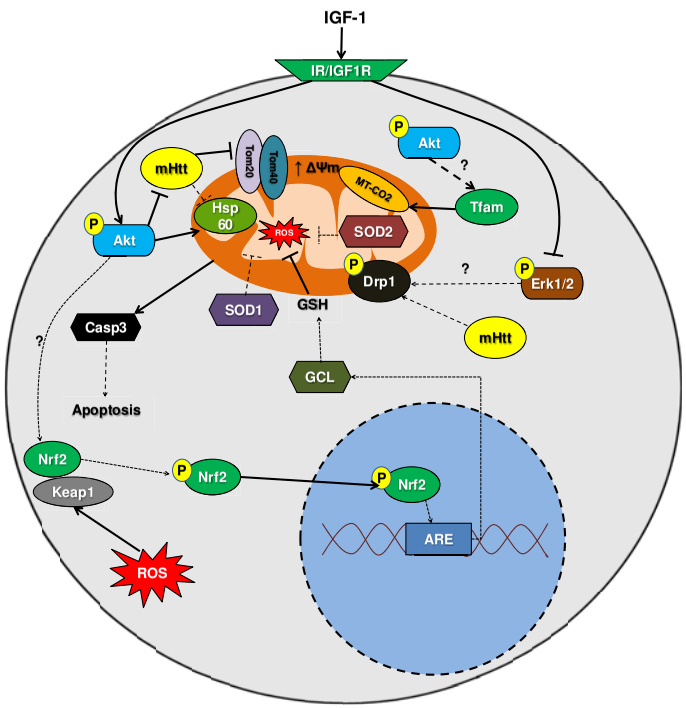
IGF-1
IR/IGF1R
mHtt
Tom20
Tom40
↑ ΔΨm
MT-CO2
Akt
Tfam
Hsp 60
ROS
SOD2
P
Akt
SOD1
GSH
Drp1
Erk1/2
Casp3
mHtt
GCL
Apoptosis
Nrf2
Keap1
Nrf2
Nrf2
ARE
ROS